UNCLASSIFIED

[redacted]

Copy 69 NACA

RM A54H23

NACA RM A54H23

CASE FILE COPY

NACA

GROUP 4
Downgraded at 3 year intervals; declassified after 12 years

RESEARCH MEMORANDUM

COMPARISON OF EXPERIMENTAL AND THEORETICAL NORMAL-FORCE DISTRIBUTIONS (INCLUDING REYNOLDS NUMBER EFFECTS) ON AN OGIVE-CYLINDER BODY AT MACH NUMBER 1.98

By Edward W. Perkins and Leland H. Jorgensen

Ames Aeronautical Laboratory
Moffett Field, Calif.

Classification Changed to UNCLASSIFIED	
Authority DOD DIR. 5200.10	
Date AUG 19 1967	By N. Devereux/M

[redacted]

NATIONAL ADVISORY COMMITTEE
FOR AERONAUTICS
WASHINGTON
November 19, 1954

[redacted]

UNCLASSIFIED

NATIONAL ADVISORY COMMITTEE FOR AERONAUTICS

RESEARCH MEMORANDUM

COMPARISON OF EXPERIMENTAL AND THEORETICAL NORMAL-FORCE DISTRIBUTIONS (INCLUDING REYNOLDS NUMBER EFFECTS) ON AN OGIVE-CYLINDER BODY AT MACH NUMBER 1.98

By Edward W. Perkins and Leland H. Jorgensen

SUMMARY

Normal-force and pressure distributions have been determined for a body of revolution consisting of a fineness-ratio-3, circular-arc, ogival nose tangent to a cylindrical afterbody 7 diameters long. The free-stream Mach number was 1.98; the angle-of-attack range was from 0° to 20°; and the Reynolds numbers, based on body diameter, were 0.15×10^{6} and 0.45×10^{6}.

Comparisons of experimental and theoretical distributions of pressure and normal-force coefficients indicate that available theoretical methods can be expected to predict experimental results with good accuracy for angles of attack only to about 5°. The zero-lift pressure distribution is adequately predicted by Van Dyke's second-order theory.

The normal-force distributions differ significantly from those calculated in accordance with theories which include methods of estimating the effects of viscosity on the forces and moments for inclined bodies. Analysis of the data shows that these differences are, in general, attributable to inadequate estimates of the magnitude and distribution of the cross forces resulting from flow separation. Results of the tests at different Reynolds numbers show that, insofar as the viscous cross-force distribution on an inclined body is concerned, the boundary-layer flow in the axial and crossflow directions cannot always be considered independent.

INTRODUCTION

The design of missiles and airplanes for operation at very high speeds, coupled with the requirement of good maneuverability, has led to the use of configurations in which the aerodynamic characteristics of the

bodies are important. Although several theoretical methods based upon potential-flow concepts are available for predicting the characteristics of bodies, the angle-of-attack range for which these theories yield satisfactory results is known to be very limited because of the effects of viscosity. An approximate theory based upon the idea that the effects of viscosity on the forces and moments for high fineness ratio bodies of revolution can be estimated by treating each cross section of the body as an element of an infinitely long circular cylinder was proposed by Allen in reference 1. Although the actual flow about an inclined body was known to be more complex than that assumed as the basis for this method, it has been shown that for many cases, the method can be used to predict satisfactorily the forces for high fineness ratio bodies (ref. 2). However, because of the assumptions involved in the development of the method, satisfactory estimates of the aerodynamic characteristics of low fineness ratio bodies cannot be expected. Furthermore, Reynolds number effects on the forces and moments are only qualitatively predicted with this method.

Studies of the flow about inclined bodies by means of the vapor-screen technique (ref. 2) have shown that there is a similarity between the axial development of the crossflow about an inclined body and the development with time of the flow about a circular cylinder impulsively set in motion from rest. Based upon this observation, it was suggested in reference 2 that the axial distribution of the crossflow drag for an inclined body may be similar to the time-dependent drag of the circular cylinder impulsively set in motion from rest. Employing this concept, Kelly (ref. 3) showed that some improvement in the estimation of the force characteristics for low fineness ratio bodies can be obtained. However, this approach yields unsatisfactory predictions for high fineness ratio bodies at large angles of attack.

Because of the lack of experimental data on the load distributions for inclined bodies, it is generally impossible to determine a priori the reasons for failure of either Allen's or Kelly's method in any particular case. It was the purpose of the present investigation to determine experimentally the normal-force distributions on an inclined body and to compare these distributions with those computed with the methods proposed in references 1 and 3. The results of these comparisons are presented in this report and are used to indicate the conditions for which the proposed methods may be expected to yield satisfactory estimates of the over-all forces and moments and those for which serious errors in the force predictions may result.

The scope of the present investigation is limited in that detailed force-distribution data for only one body were obtained for analysis. Nevertheless, it is felt that the results are generally indicative of the conditions which might exist for a wide variety of cases. Since it was necessary to obtain pressure-distribution data in order to determine the

force distributions, pressure distributions are also presented and compared with the predictions of potential theories.

SYMBOLS

A reference area, πd^2

c_{d_c} local crossflow drag coefficient based on diameter

c_{d_c}' crossflow drag coefficient of a circular cylinder per unit length in terms of its diameter for steady-state flow

C_m pitching-moment coefficient about nose of the model,

$$\frac{M}{q_o A d} = -\frac{1}{d}\int_0^l c_n\, x\, dx$$

c_n local normal-force coefficient per unit length, $\frac{2r}{A}\int_0^\pi C_p \cos\theta\, d\theta$

C_N total normal-force coefficient, $\int_0^l c_n\, dx$

C_p pressure coefficient, $\frac{p - p_o}{q_o}$

d maximum body diameter

l body length

l_m axial distance from vertex to station at which local normal force by "hybrid" or Tsien's theory is a minimum

l_n length of ogival nose

M pitching moment

M_o free-stream Mach number

M_c crossflow Mach number, $M_o \sin\alpha$

p local static pressure on model surface

p_o free-stream static pressure

q_o free-stream dynamic pressure

Re free-stream Reynolds number per inch

Re_c crossflow Reynolds number based on body diameter (Re d sin α)

x,r,θ model cylindrical coordinates, origin at the vertex ($\theta = 0^{\circ}$ in the vertical plane of symmetry on the windward side)

x_m moment center location measured from vertex

x_p center-of-pressure location measured from vertex

α angle of attack

Subscripts

p potential-flow component

v viscous-flow component

APPARATUS AND TESTS

Tunnel

The experimental investigation was conducted in the Ames 1- by 3-foot supersonic wind tunnel No. 1. This tunnel is a closed-circuit variable-pressure tunnel in which the Reynolds number is changed by varying the total pressure within the approximate limits of one-fifth of an atmosphere to two atmospheres. Mach numbers between 1.2 and 2.5 are obtained by adjustment of the upper and lower flexible steel plates of the nozzle.

Model

The model tested had a fineness-ratio-3 tangent ogive nose with a cylindrical afterbody. A single row of 23 orifices extended longitudinally over both nose and afterbody. The model, which was constructed of steel, was sting supported from the rear and could be rotated 360° about its longitudinal axis by a mechanism operated from outside the tunnel. Pertinent model dimensions and orifice locations are presented in figure 1.

Tests

The pressure-distribution data were obtained for a Mach number of 1.98. The model was tested at angles of attack of 0°, 5°, 10°, 15°, and 20° for a free-stream Reynolds number of 0.39×10^6 per inch and at angles of attack of 10° and 15° for a free-stream Reynolds number of 0.13×10^6 per inch (Reynolds numbers of 0.45×10^6 and 0.15×10^6 based on body diameter). At each angle of attack, circumferential pressure distributions were obtained by rotating the model through the desired range of circumferential angles (θ) in increments of 15° or less. All pressures were photographically recorded from a multiple-tube manometer system.

Since the pressure-distribution data were obtained from a single longitudinal row of orifices by rotating the model so that the orifices were in the desired plane, a check was made to determine if hysteresis effects resulted from this testing method. Comparisons of the pressure distributions (fig. 2) show that, even though there were small asymmetries in the flow, there were no effects of hysteresis due to model rotation.

In addition to the hysteresis check, a repeat run for $\alpha = 15^\circ$ and Re = 0.39×10^6 per inch was made at a later date. A comparison of the pressure-distribution data from this run with the data from the "hysteresis run" (fig. 2) indicates that the pressure distributions can be repeated with good accuracy except, as expected, near the positions of flow separation.

To help assess the effects of Reynolds number and transition from laminar to turbulent flow on the pressure and normal-force distributions, the model was also tested at 0°, 15°, and 20° angles of attack with a turbulence-producing grid mounted upstream of the wind-tunnel throat at about the 0.5 Mach number position. From schlieren pictures of the model at 0° angle of attack, it was found that for a free-stream Reynolds number of 0.39×10^6 per inch, use of the turbulence grid resulted in forward movement of the transition position from 7.5 body diameters to 6 body diameters from the vertex.

REDUCTION OF DATA

All the data have been reduced to pressure-coefficient form and have been corrected for the effects of the small nonuniformities in the wind-tunnel flow. The corrected pressure coefficients are listed in table I. For the model at zero angle of attack, an average value of C_p is listed for each x/d station, since the variation of C_p around the body was less than ±0.002.

For the model at angle of attack, local normal-force coefficients (c_n) were obtained by integrating the pressure coefficients around half of the body. Although some of the pressure distributions were slightly asymmetric, it was found that negligible error in c_n resulted from the assumption of symmetrical flow. The local normal-force data were then graphically integrated to obtain total normal-force and pitching-moment coefficients.

The uncertainty of the experimental data was estimated by considering the possible errors in the individual measurements (including corrections) used in the calculation of the final results. The uncertainty of a quantity was taken as the square root of the sum of the squares of the possible errors in the individual measurements. The resulting uncertainties in the final quantities are as follows:

Quantity	Uncertainty
C_p	±0.005
c_n	±.004
C_N	±.008
C_m	±.055
α	±.1°

Except near the regions of flow separation, the computed uncertainty in C_p appears to be consistent with the repeatability of the data. (See, e.g., fig. 2.)

RESULTS AND DISCUSSION

Pressure Distributions

Comparison of theoretical and experimental pressure distributions.- Most of the comparisons of the theoretical pressure distributions with the experimental data which are made in the figures of this report are for a Reynolds number of 0.39×10^6 per inch. Comparisons at a single Reynolds number are considered sufficient since, for zero angle of attack, the Reynolds number effects are negligible, and for angle of attack, varying the Reynolds number alters the details of the pressure distributions but does not significantly change the agreement with theory.

Theoretical pressure distributions at zero angle of attack, calculated with four different methods (refs. 4, 5, and 6) are compared with the experimental results in figure 3. Except near the vertex, the pressure distributions predicted with the various theories do not differ appreciably and are in good agreement with experiment. Of the three theoretical methods which yield satisfactory agreement over the full

length of the nose, that is, the method of characteristics, Van Dyke's second-order theory, and the method of Bolton-Shaw and Zienkiewicz, the last (ref. 5) is by far the simplest to use.

Of the several theoretical methods available for calculating the pressure distributions on inclined bodies of revolution, two have been chosen for comparison with the experimental results. These are the familiar first-order theory and the so-called "hybrid" theory of reference 7.[1] This latter method combines a first-order crossflow solution with a second-order axial-flow solution. The theoretical pressure distributions along meridian lines (θ = constant), computed with hybrid theory, are compared with the experimental distributions for angles of attack of 5°, 10°, 15°, and 20° in figure 4. The distributions obtained with first-order theory are shown only for $\alpha = 10^\circ$ since, except near the vertex, there is little difference between the results of first-order theory and hybrid theory. For all angles of attack and for most values of θ, the hybrid theory predicts too large a value of the pressure coefficient at the vertex of the model. Good agreement of theory with experiment over most of the body is obtained only at 5° angle of attack, the differences between theory and experiment becoming progressively greater as the angle of attack is increased. Because of the excellent agreement between second-order theory and experiment at zero angle of attack, the failure of the hybrid theory, even for moderate angles of attack, is probably attributable to inaccuracies inherent in the first-order crossflow contribution. Flow separation, which occurs at all but the lowest angle of attack, is the principal cause of the poor agreement over the leeward side of the cylindrical afterbody.

Effects of angle of attack on the pressure distributions.- In order to show more clearly the effects of angle of attack on the variation of pressure coefficient around the body, circumferential pressure distributions for six axial stations are presented in figure 5. At all angles of attack above 5°, effects of crossflow separation are indicated. As the angle of attack increases from 5° to 10°, a separated flow region is formed aft on the lee side of the body. With further increase in angle of attack, the separated flow region moves forward and also progresses toward the windward side of the body until it encompasses almost the entire lee side at 20° angle of attack. On the lee side of the body, in this separated flow region, secondary flow effects associated with the body vortices are also observed. (See, e.g., fig. 5(c) at $\alpha=20^\circ$ and $\theta \approx 150^\circ$.) There is also evidence of slight flow asymmetry on the lee side of the body.

Reynolds number effects on the pressure distributions.- The effects of Reynolds number on the pressure distributions result principally from the changes in the boundary-layer-separation characteristics and thus

[1]In the application of both theories, the exact pressure relationship for isentropic flow has been used.

depend primarily on whether the boundary layer is laminar or turbulent. Since an increase in the turbulence level of an air stream is known to induce effects which are qualitatively similar to those resulting from an increase in Reynolds number, an effectively high Reynolds number was achieved by purposely increasing the free-stream turbulence and testing at the highest practicable tunnel total pressure. The pressure distributions obtained under these conditions, combined with the data obtained at low tunnel pressures in the absence of the turbulence grid, provide a fairly wide range of effective Reynolds numbers.

The data of figure 6 illustrate the Reynolds number or boundary-layer transition effects on the pressure distributions for the body of the present investigation. The data have been plotted for six stations along the length of the body and for angles of attack of 10°, 15°, and 20°. Large Reynolds number effects are evidenced only by the data for 10° angle of attack. For the higher angles of attack, 15° and 20°, Reynolds number effects are present but they are much less pronounced.

The changes in the pressure distributions on the cylindrical afterbody which accompany the increase in Reynolds number at 10° angle of attack (fig. 6(a)) are qualitatively the same as those which result from boundary-layer transition on a circular cylinder. For a circular cylinder, when boundary-layer transition occurs ahead of the point at which laminar separation would usually occur, the separation point moves toward the lee side of the cylinder and the pressure recovery on the lee side increases. On the cylindrical afterbody of the model of the present investigation, the increase in Reynolds number from 0.13×10^{6} per inch to 0.39×10^{6} per inch is accompanied by a movement of the flow separation point toward the lee side of the body and an increase in the lee side pressure recovery. From these data it is inferred that for $Re = 0.39\times10^{6}$ at $\alpha = 10^{\circ}$, boundary-layer transition occurred on the inclined body near the juncture of the nose with the cylindrical afterbody.

Normal-Force Distributions

<u>Comparison with potential theory</u>.- Normal-force distributions for angles of attack of 5°, 10°, 15°, and 20° for a Reynolds number of 0.39×10^{6} per inch are presented in figure 7. The experimental data have been reduced to the form of local normal-force coefficient per unit angle of attack for convenient comparison with the theoretical distributions calculated with slender-body theory, Tsien's linearized theory and Van Dyke's hybrid theory[2] (refs. 8, 9, and 7, respectively). The inadequacy of the

[2]Although the theoretical normal force calculated with Van Dyke's hybrid theory is not strictly a linear function of the angle of attack, for this particular combination of body shape and Mach number, the departure from linearity is negligibly small for the angle-of-attack range of this investigation.

potential-flow theories at all but very low angles of attack is clearly demonstrated by these comparisons. Even at 5° angle of attack it is evident that, although both Tsien's and Van Dyke's methods predict the general shape of the load distribution curve, the lift carried on the cylindrical afterbody is considerably greater than calculated. At higher angles of attack the largest part of the difference between theory and experiment is attributable to separation effects.

Comparison with methods of Allen and Kelly.- In the absence of a rigorous theory for calculating the effects of flow separation on the forces and moments of inclined bodies, methods of estimating these effects have been suggested by Allen (ref. 1) and Kelly (ref. 3). Although both methods rely upon the same concept, that is, that the viscous crossflow around an inclined body of revolution is analogous to the flow around a circular cylinder normal to the air stream, the methods differ in their subsequent development. In Allen's method it is assumed that the local viscous cross force depends only upon the component of flow normal to the inclined axis of the body. Therefore, no interaction between the axial and crossflow boundary layers is anticipated. The local viscous crossflow drag coefficient is assumed constant along the body and is taken as equal to the drag coefficient of a circular cylinder of the same fineness ratio as the inclined body and at the same crossflow Mach number and Reynolds number.

Two modifications to Allen's method are suggested by Kelly (ref. 3). First, it is assumed that the viscous crossflow and axial flow are not independent. Thus, if the boundary-layer flow on the body is turbulent for any reason whatsoever, the appropriate crossflow drag coefficient is the low value associated with turbulent boundary-layer flow, even though the crossflow Reynolds number might be in the range for which a laminar crossflow boundary layer would be expected. (Kelly does not consider cases for which the boundary-layer flow is partly laminar and partly turbulent.) The second modification is that, at any angle of attack, the crossflow drag coefficient should not be constant along the length of the body but should reflect the transient effects noted by Schwabe (ref. 10) for a circular cylinder impulsively set in motion from rest. Schwabe's data show that the drag coefficient starts at zero at zero time and increases with distance traveled, until a maximum value of approximately 2.07 is reached after the cylinder has traveled about 4.5 diameters. Thus, based on the assumption that the crossflow drag coefficients of a circular cylinder and an inclined body would be equal for equal distances traveled in the respective crossflow planes, the axial variation for an inclined body was related to the variation with distance traveled of the drag coefficient of a circular cylinder.

Although both Allen's and Kelly's methods have been shown to yield satisfactory predictions of the over-all forces and moments with angle of attack for a number of specific cases, neither method yields satisfactory

results in every instance. The reasons for the failure of the approximate methods can be traced to the fact that the actual distribution of the forces differs significantly from those assumed. For the model tested in the present investigation, this is illustrated in figure 8 by the comparisons of the normal-force distributions calculated by Allen's and Kelly's methods with the distributions determined by integration of the pressure-distribution data. The experimental data include the results obtained for two values of the Reynolds number, as well as the data obtained with the turbulence grid installed in the tunnel. From the comparisons it is evident that the distributions estimated on the basis of either Allen's or Kelly's method are not in good agreement with the experimentally determined distributions for the complete angle-of-attack range. Hence, although either method may yield fairly accurate estimates of the total normal force, because of the failure to predict accurately the distribution, neither method can be expected to yield the correct pitching moment and center-of-pressure position.

Crossflow-drag-coefficient distributions.- It is believed that the major source of error in the loadings calculated with the approximate methods is the inadequate estimates of the forces resulting from flow separation. With the assumption that the potential-flow forces are correctly predicted with theory and that the differences between experiment and potential theory are attributable to flow separation effects, longitudinal distributions of the effective[3] local crossflow drag coefficients may be obtained from the data. These distributions are compared with the distributions assumed in Allen's and Kelly's methods in figure 9. It is apparent that neither of the proposed methods contains the essential features of the experimental distributions. Although there are differences between the experimental distributions for different Reynolds numbers and angles of attack (these will be discussed later), in each case the effective crossflow drag coefficient starts near zero at the apex, rises to a maximum value downstream from the juncture of the nose with the cylindrical afterbody, and then decreases. In contrast with this characteristic distribution, in Allen's method it is assumed that the crossflow drag coefficient is constant along the length of the body. It is apparent that Allen's method provides a first approximation to the total additional cross force attributable to viscous effects, but that, as was pointed out in reference 2, the centroid of this added loading is too far forward, with the consequence that the actual center of pressure is more rearward than the viscous theory indicates.

The distribution of crossflow drag coefficient computed with Kelly's method is in qualitative agreement with experimental results in that it

[3]These coefficients have been termed "effective" crossflow drag coefficients because all of the difference between potential theory and experiment may not be attributed reasonably to viscous effects alone. Particularly at the larger angles of attack, some of the difference must be chargeable to failure of the potential theory itself.

starts at a low value near the apex and increases with distance downstream. However, the experimental data reach a maximum value at 2 to 3 diameters downstream of the ogive-cylinder juncture and thereafter decrease; whereas, Kelly's assumed distribution continues to increase for the full length of the body. It is evident that the use of Kelly's method, as compared with Allen's, results in a rearward shift of the center-of-pressure position and, for the angles of attack shown, an increase in the total normal force. As will be shown subsequently, both of these effects result in improved agreement with the experimental normal forces and pitching moments for the angle-of-attack range investigated.

Comparison of the experimental and assumed distribution of the crossflow drag coefficient at 20° angle of attack (fig. 9) shows that Kelly's method assumes much too large a value beyond about 6 diameters downstream from the nose vertex. This results in too large a value of normal force and a center-of-pressure position too far aft. For bodies with longer cylindrical afterbodies or bodies of higher fineness ratio this overestimation of the cross force on the afterbody leads to large errors in the estimated characteristics. It is, therefore, clear why Kelly's method yields good estimates of the over-all viscous effects for low fineness ratio bodies for perhaps a relatively large angle-of-attack range but, in general, does not yield good estimates for high fineness ratio bodies at large angles of attack. A word of warning should be extended at this point. Although it is stated in reference 3 that the method suggested therein is applicable as long as the value of $l/d \tan \alpha$ does not exceed 4.5, it appears from the load distribution data (fig. 8) that, at least for the model tested in this investigation, large errors in the predicted characteristics result if the method is used for values of $l/d \tan \alpha$ greater than about 2.7 ($l/d = 10$, $\alpha = 15^\circ$).

Reynolds number effects.- For the body tested in the present investigation, the Reynolds number effects on the normal-force distribution and on the distribution of the effective crossflow drag coefficient are shown in figures 8 and 9, respectively. At 10° angle of attack, a large decrease in the local cross force on the cylindrical afterbody accompanied an increase in the Reynolds number from 0.13×10^6 to 0.39×10^6 per inch. As previously indicated in the discussion of the pressure distribution data, this reduction in cross force evidently results from the effects of boundary-layer transition.

The reduction of the Reynolds number effect with increasing crossflow Mach number (increasing angle of attack), shown by the experimental data, is in accord with the expected trend based upon the analogy with the crossflow around a circular cylinder. For the circular cylinder it is known that the Reynolds number effects decrease as the Mach number increases. For the inclined body the Mach number normal to the axis of the body was 0.34 at $\alpha = 10^\circ$ and increased to 0.51 at $\alpha = 15^\circ$. The data show that, whereas a large decrease in the local crossflow drag coefficient accompanied boundary-layer transition at $\alpha = 10^\circ$, for the same free-stream Reynolds number change at $\alpha = 15^\circ$, the decrease in the local

crossflow drag coefficient was much less. In fact, further increases in the effective Reynolds number through the use of the turbulence grid resulted in little change in the crossflow drag coefficient.

These data show that the "independence principle," whereby the viscous crossflow and axial flow are considered independent of each other, is not always applicable. Hill, in reference 11, suggested the inadequacy of this principle for cases in which boundary-layer transition occurs on an inclined body. If the independence principle were always applicable, then for each angle of attack, the local viscous crossflow drag coefficient would be a function only of the crossflow Reynolds number. Thus, for each angle of attack, there should be a consistent difference between the distributions for two different Reynolds numbers (fig. 9). However, the data for 10° and 15° angle of attack show that the distributions for both Reynolds numbers are about the same over the first few body diameters, but for stations farther downstream, the values of crossflow drag coefficient are lower for the higher Reynolds number.

It is clear, therefore, that the local crossflow drag coefficient depends on whether the boundary layer is laminar or turbulent and is not determined only by the crossflow Reynolds number and Mach number. Hence, for an accurate estimate of the viscous cross-force distribution, it is necessary to know the position of boundary-layer transition. It is apparent that neither Allen's nor Kelly's method can account for the observed Reynolds number effects, since each uses what might be termed a universal loading curve to represent the longitudinal distribution of crossflow drag coefficient, with Reynolds number effects taken into account by simple multiples of these curves.

Correlation of crossflow drag distributions.- From figure 9 it is observed that, except for the high Reynolds number data at $\alpha = 10^\circ$, the axial distributions of the effective crossflow drag coefficient (c_{d_c}) at each angle of attack are similar. This similarity suggests that the data might be correlated by dividing the ordinate c_{d_c} by the cylinder steady-state value c_{d_c}' (ref. 12) which would be expected far downstream on an extended afterbody. However, as anticipated, it was found that only the data evidencing little or no effects of Reynolds number could be approximately correlated to a single curve (cf. figs. 10(a) and 10(b)). Because boundary-layer transition apparently occurred near the nose-cylinder juncture for the model at 10° angle of attack and $Re = 0.39 \times 10^6$ per inch, these data depart significantly from the single correlation curve. For angles of attack of 15° and 20°, the deviations of the data from the correlation curve are not large, even though Reynolds number variations are present. It is therefore apparent that the single correlation curve represents the data satisfactorily only for conditions in which either the boundary layer is laminar or the Mach number normal to the body axis is greater than about 0.5.

The development of a general correlation curve from which the viscous cross-force distribution for bodies of revolution could be computed

readily would provide the designer with a very powerful tool. Unfortunately the correlation curve developed from the foregoing data may be used only for bodies with geometrically similar nose shapes and with cylindrical afterbodies. Although there are not sufficient data available from which the effects of all the significant parameters of the problem can be determined, an indication of the manner in which the effects of nose fineness ratio may be taken into account in the correlation is provided from figures 7 and 10 of the present report. The maximum positive value of c_{d_c}/c_{d_c}' and the maximum negative value of the theoretical potential-flow cross force occur at approximately the same longitudinal position.[4] This fact suggests that the effect of nose fineness ratio on the longitudinal distribution of the effective viscous cross force might be satisfactorily accounted for by using l_m (the distance from the apex of the body to the position of the minimum value of the theoretical potential-flow cross force) as the unit of length rather than simply the distance in body diameters as used in figure 10. Accordingly, the correlation curve has been replotted in figure 11 for comparison with similar data for a fineness ratio 5.75 ogive plus cylindrical afterbody (ref. 13).[5] It is evident that a satisfactory correlation results.

Although the correlations obtained with these data have only limited applicability, it is hoped that they will provide a suitable framework for further correlations when additional data become available. It should be noted that l_m is a function of both nose fineness ratio and free-stream Mach number and might, therefore, provide a correlation with respect to the Mach number effects for a given body.

Normal-Force and Pitching-Moment Characteristics

Normal-force, pitching-moment, and center-of-pressure characteristics obtained by graphical integration of the experimental normal-force distributions of figure 8 are presented in figures 12 and 13. A considerable reduction in normal force and a forward shift of the center-of-pressure position accompanied the increase in Reynolds number at $\alpha = 10^{\circ}$. Similar changes, although of reduced magnitude, occurred at $\alpha = 15^{\circ}$ and $\alpha = 20^{\circ}$. These experimental characteristics are compared with those predicted by the semiempirical methods of Allen (ref. 1) and Kelly (ref. 3). Also included for reference are the characteristics

[4]This is, of course, not unexpected, since the correlation curves were derived through the use of the theoretical potential cross-force distributions.

[5]The data of reference 13 were also obtained from the Ames 1- by 3-foot supersonic wind tunnel No. 1 at the same Mach number of 1.98.

predicted with potential theories alone (refs. 7 and 9) and with the correlation curve (fig. 11) according to the procedure outlined in the Appendix of this report. In the application of Allen's method, the steady-state values of crossflow drag coefficient (c_{d_c}') are taken as functions of the crossflow Reynolds numbers and crossflow Mach numbers and, hence, vary with angle of attack. In the application of Kelly's method, c_{d_c}' is taken as 1.2 or 0.35, depending on whether the boundary layer is laminar or turbulent. These comparisons show that none of the methods used can be considered satisfactory for all of the test conditions. For the cases in which the boundary layer is known to be laminar, that is the tests for $Re = 0.13 \times 10^6$ per inch at α's of 10° and 15°, the values predicted with Kelly's method and with the correlation curve are both in reasonably good agreement with the experimental data. For the remaining experimental data the boundary layer was turbulent over at least a part of the body. If the method suggested by Kelly is used, with his value of $c_{d_c}' = 0.35$ for a turbulent boundary layer, both the normal force and pitching moment are grossly underestimated at the higher angles of attack.

CONCLUDING REMARKS

A study of the effects of viscosity on the normal-force distributions for an ogive-cylinder body of revolution of fineness ratio 10 has been conducted. The free-stream Mach number was 1.98. The angle-of-attack range was 0° to 20°, and the Reynolds numbers, based on body diameter, were 0.15×10^6 and 0.45×10^6. A Reynolds number effectively higher than 0.45×10^6 was obtained by using a turbulence inducing grid in the entrance to the wind-tunnel nozzle.

The experimental data show that, insofar as the viscous cross-force distribution on an inclined body is concerned, if transition of the boundary layer occurs, the crossflow cannot be considered to be independent of the axial flow for crossflow Mach numbers less than about 0.6. This is true, in spite of the fact that the crossflow Reynolds number may be much lower than that at which transition of the crossflow boundary layer would be expected. Upstream of the transition point the crossflow characteristics are those associated with a laminar boundary layer, while downstream the crossflow characteristics approach those associated with a turbulent boundary layer.

The distributions of viscous crossflow drag coefficients, determined from the differences between the experimentally determined normal-force distributions and the distributions predicted with potential-flow theory, differ considerably from the distributions assumed in either of the methods which have been proposed for estimating the effects of viscosity on the forces and moments of inclined bodies of revolution (Allen,

NACA RM A9I26 and Kelly, NOTS TM-998). A correlation curve for the longitudinal distribution of the crossflow drag coefficient for laminar boundary-layer flow was developed, based upon the assumption that the distribution depended only upon the body shape. It is believed that use of this correlation curve for the viscous cross-force contribution in conjunction with first-order linear theory for the potential cross force provides a satisfactory method for estimating the normal-force and pitching-moment characteristics for similarly shaped bodies of revolution with laminar boundary-layer flow. Additional study is required to determine the Mach number range for which the correlation curve is applicable.

Ames Aeronautical Laboratory
National Advisory Committee for Aeronautics
Moffett Field, Calif., Aug. 20, 1954

APPENDIX

PROCEDURE FOR USE OF THE CORRELATION CURVE IN COMPUTING NORMAL-FORCE AND PITCHING-MOMENT COEFFICIENTS

A simple procedure by which the aerodynamic characteristics of bodies similar to that studied in the present investigation may be computed is summarized in the following steps:

(1) Compute potential-flow distribution (c_{n_p} vs. x) using Van Dyke's "hybrid" or Tsien's potential theory.

(2) Determine l_m, the axial distance from the vertex to the "x" station at which c_{n_p} is a minimum according to potential theory.

(3) For various "x" stations, determine the corresponding values of c_{d_c}/c_{d_c}' using figure 11.

(4) For values of $M_o \sin\alpha$, determine the corresponding values of c_{d_c}' using reference 12.

(5) Compute the viscous components of the total normal-force and pitching-moment coefficients by graphically solving the equations,

$$C_{N_v} = \frac{2\, c_{d_c}' \sin^2\alpha}{A} \int_0^l r\left(\frac{c_{d_c}}{c_{d_c}'}\right) dx$$

$$C_{m_v} = \frac{2\, c_{d_c}' \sin^2\alpha}{Ad} \int_0^l r\left(\frac{c_{d_c}}{c_{d_c}'}\right) (x_m - x)\, dx$$

(6) Compute the potential components of the total normal-force and pitching-moment coefficients by graphically integrating the c_{n_p} distributions of step (1).

$$C_{N_p} = \int_0^l c_{n_p}\, dx$$

$$C_{m_p} = \frac{1}{d} \int_0^l c_{n_p} (x_m - x)\, dx$$

(7) The total normal-force and pitching-moment coefficients are then obtained by direct addition of the viscous and potential components, that is,

$$C_N = C_{N_p} + C_{N_v}$$

$$C_m = C_{m_p} + C_{m_v}$$

REFERENCES

1. Allen, H. Julian: Estimation of the Forces and Moments Acting on Inclined Bodies of Revolution of High Fineness Ratio. NACA RM A9I26, 1949.

2. Allen, H. Julian, and Perkins, Edward W.: Characteristics of Flow Over Inclined Bodies of Revolution. NACA RM A50L07, 1951.

3. Kelly, Howard R.: The Estimation of Normal Force and Pitching Moment Coefficients for Blunt-Based Bodies of Revolution at Large Angles of Attack. Naval Ordnance Test Station, Inyokern, Calif. Tech. Memo. 998, 27 May 1953.

4. Rossow, Vernon J.: Applicability of the Hypersonic Similarity Rule to Pressure Distributions Which Include the Effects of Rotation for Bodies of Revolution at Zero Angle of Attack. NACA TN 2399, 1951. (Extension of NACA TN 2250)

5. Bolton-Shaw, B. W., and Zienkiewicz, H. K.: The Rapid, Accurate Prediction of Pressure on Non-Lifting Ogival Heads of Arbitrary Shape at Supersonic Speeds. English Electric Company, Navigational Project Division. No. L.A.t. 034 (British), 23 June 1952.

6. Van Dyke, Milton D.: Practical Calculation of Second-Order Supersonic Flow Past Nonlifting Bodies of Revolution. NACA TN 2744, 1952.

7. Van Dyke, Milton D.: First- and Second-Order Theory of Supersonic Flow Past Bodies of Revolution. Jour. Aero. Sci., vol. 18, no. 3, Mar. 1951, pp. 161-178, 216.

8. Munk, Max. M.: The Aerodynamic Forces on Airship Hulls. NACA Rep. 184, 1924.

9. Tsien, Hsue-Shen: Supersonic Flow Over an Inclined Body of Revolution. Jour. Aero. Sci., vol. 5, no. 12, Oct. 1938, pp. 480-483.

10. Schwabe, M.: Pressure Distribution in Nonuniform Two-Dimensional Flow. NACA TM 1039, 1943.

11. Hill, J. A. F.: Forces on Slender Bodies at Angles of Attack. Mass. Inst. of Tech., Naval Supersonic Laboratory, R-a 100-59, May 9, 1950.

12. Gowen, Forrest E., and Perkins, Edward W.: Drag of Circular Cylinders for a Wide Range of Reynolds Numbers and Mach Numbers. NACA TN 2960, 1953. (Formerly NACA RM A52C20)

13. Perkins, Edward W., and Kuehn, Donald M.: Comparison of the Experimental and Theoretical Distributions of Lift on a Slender Inclined Body of Revolution at M = 2. NACA RM A53E01, 1953.

TABLE I.- EXPERIMENTAL PRESSURE COEFFICIENTS FOR MODEL AT VARIOUS ANGLES OF ATTACK AND REYNOLDS NUMBERS; $M_0 = 1.98$

(a) $\alpha=0^{\circ}$, $Re=0.39\times10^{6}$ per inch

$\frac{x}{d}$	0.22	0.56	0.89	1.22	1.61	2.06	2.5	2.95	3.62	4.06	4.50	5.39	6.28	7.17	8.06
C_p	0.260	0.212	0.165	0.115	0.074	0.026	-0.014	-0.038	-0.030	-0.017	-0.012	-0.009	-0.001	0.000	0.006

(b) $\alpha=5^{\circ}$, $Re=0.39\times10^{6}$ per inch

$\frac{x}{d}$	Radial angle, θ, deg																										
	0	15	30	45	60	75	90	105	120	135	140	145	150	155	160	165	170	175	180	185	190	200	210	220	240	255	270
0.22	0.351	0.347	0.335	0.317	0.295	0.269	0.245	0.224	0.205	0.191	0.188	0.181	0.181	0.179	0.178	0.177	0.177	0.177	0.176	0.175	0.178	0.178	0.182	0.188	0.206	0.225	0.247
.56	.299	.295	.284	.266	.245	.220	.197	.177	.160	.148	.145	.139	.139	.138	.136	.135	.135	.134	.134	.134	.136	.137	.142	.146	.162	.179	.199
.89	.239	.236	.226	.209	.189	.167	.145	.128	.113	.102	.100	.094	.094	.094	.092	.092	.092	.092	.092	.091	.092	.093	.097	.100	.111	.126	.143
1.22	.188	.184	.176	.161	.143	.123	.103	.088	.075	.066	.065	.061	.061	.060	.059	.059	.058	.059	.058	.057	.058	.058	.060	.062	.071	.084	.100
1.61	.131	.129	.122	.109	.094	.076	.060	.047	.036	.029	.027	.024	.024	.023	.022	.022	.021	.021	.021	.020	.021	.021	.022	.024	.031	.041	.054
2.06	.071	.068	.062	.052	.039	.024	.011	.001	-.007	-.013	-.014	-.016	-.017	-.018	-.018	-.018	-.019	-.019	-.020	-.020	-.020	-.020	-.020	-.019	-.012	-.005	.004
2.50	.019	.018	.012	.003	-.009	-.022	-.033	-.041	-.047	-.050	-.049	-.050	-.050	-.050	-.050	-.049	-.049	-.049	-.049	-.050	-.049	-.050	-.051	-.052	-.052	-.046	-.038
2.95	-.013	-.014	-.020	-.029	-.040	-.050	-.060	-.065	-.068	-.068	-.068	-.066	-.068	-.066	-.066	-.065	-.064	-.064	-.064	-.065	-.064	-.065	-.066	-.068	-.072	-.070	-.066
3.62	-.016	-.017	-.021	-.029	-.039	-.049	-.055	-.056	-.055	-.053	-.051	-.050	-.050	-.049	-.049	-.047	-.047	-.047	-.047	-.048	-.047	-.048	-.050	-.053	---	---	---
4.06	-.014	-.015	-.020	-.028	-.037	-.046	-.051	-.049	-.046	-.044	-.043	-.041	-.041	-.040	-.040	-.038	-.037	-.036	-.036	-.036	-.036	-.040	-.043	-.046	-.051	-.056	-.057
4.50	-.008	-.009	-.014	-.023	-.033	-.041	-.046	-.044	-.039	-.037	-.036	-.034	-.034	-.032	-.030	-.027	-.025	-.024	-.024	-.024	-.024	-.029	-.036	-.040	-.046	-.048	-.050
4.95	-.009	-.010	-.016	-.024	-.033	-.040	-.044	-.042	-.043	-.040	-.038	-.032	-.032	-.028	-.024	-.021	-.019	-.017	-.017	-.017	-.016	-.018	-.019	-.026	-.036	-.041	-.042
5.39	-.008	-.011	-.015	-.019	-.028	-.036	-.040	-.038	-.035	-.029	-.027	-.018	-.017	-.015	-.013	-.012	-.011	-.010	-.009	-.009	-.008	-.010	-.015	-.024	-.033	-.042	-.047
5.84	-.001	-.003	-.012	-.019	-.025	-.032	-.036	-.034	-.026	-.017	-.015	-.010	-.010	-.007	-.005	-.004	-.004	-.004	-.005	-.005	-.006	-.008	-.013	-.017	-.021	-.029	-.035
6.28	-.005	-.003	-.006	-.016	-.027	-.033	-.034	-.029	-.021	-.015	-.012	-.009	-.009	-.006	-.004	-.002	-.001	.000	.001	---	.001	-.003	-.007	-.012	-.022	-.029	-.033
6.72	-.001	-.005	-.011	-.017	-.025	-.030	-.029	-.025	-.019	-.014	-.013	-.010	-.010	-.008	-.004	-.002	.000	.002	.002	.002	.002	-.003	-.009	-.013	-.022	-.029	-.034
7.17	-.001	-.003	-.009	-.015	-.020	-.022	-.023	-.021	-.016	-.011	-.009	-.006	-.006	-.005	-.002	.000	.001	.001	.001	---	.001	---	-.002	-.005	-.012	-.018	-.022
7.61	-.002	-.001	-.004	-.011	-.017	-.023	-.025	-.022	-.016	-.011	-.009	-.007	-.007	-.006	-.004	-.002	.000	.002	.003	.003	.003	.001	.000	-.002	-.011	-.017	-.020
8.06	.011	.007	.002	-.006	-.014	-.018	-.020	-.017	-.012	-.007	-.005	-.004	-.003	-.002	000	.003	.005	.007	.007	.007	.007	.004	.000	-.002	-.009	-.015	-.020
8.50	.017	.013	.008	-.001	-.011	-.019	-.021	-.017	-.011	-.006	-.004	-.004	-.003	-.003	-.002	-.001	.001	.001	.002	.001	.002	-.002	-.003	-.005	-.011	-.017	-.021
8.95	.016	.015	.010	.003	-.004	-.010	-.012	-.009	-.004	-.001	.001	.001	.001	.000	.001	.002	.003	.004	.004	.003	.003	.000	-.001	-.002	-.005	-.009	-.013
9.39	.017	.016	.012	.005	-.002	-.009	-.011	-.008	-.003	.001	.002	.002	.002	.002	.003	.004	.005	.005	.005	.005	.006	.004	.003	.002	-.004	-.008	-.012
9.83	.021	.019	.013	.005	-.003	-.009	-.010	-.007	-.002	.002	.003	.003	.003	.004	.004	.006	.007	.008	.009	.008	.008	.006	.005	.004	-.001	-.006	-.010

(c) $\alpha=10^{\circ}$, $Re=0.39\times10^{6}$ per inch

$\frac{x}{d}$	Radial angle, θ, deg																									
	0	15	30	45	60	75	90	105	120	135	140	145	150	155	160	165	170	175	180	190	200	210	220	240	255	270
0.22	0.471	0.459	0.428	0.382	0.327	0.270	0.216	0.172	0.143	0.125	0.122	0.118	0.117	0.116	0.115	0.115	0.114	0.115	0.115	0.113	0.115	0.117	0.122	0.146	0.178	0.226
.56	.406	.395	.367	.325	.273	.220	.170	.128	.101	.086	.082	.079	.079	.078	.077	.078	.078	.077	.078	.077	.078	.079	.083	.102	.129	.171
.89	.339	.328	.301	.261	.213	.163	.117	.080	.056	.044	.041	.040	.039	.040	.040	.040	.041	.042	.041	.041	.040	.039	.040	.052	.076	.113
1.22	.285	.272	.247	.210	.163	.117	.074	.040	.018	.010	.009	.009	.009	.010	.010	.012	.013	.013	.013	.012	.011	.009	.009	.015	.034	.068
1.61	.220	.210	.187	.154	.113	.071	.032	.001	-.016	-.022	-.022	-.022	-.021	-.020	-.020	-.018	-.017	-.016	-.016	-.017	-.018	-.021	-.023	-.022	-.008	.021
2.06	.147	.140	.120	.089	.052	.014	-.020	-.046	-.061	-.057	-.056	-.054	-.052	-.050	-.049	-.046	-.046	-.045	-.045	-.047	-.050	-.054	-.058	-.061	-.052	-.029
2.50	.084	.077	.059	.030	-.004	-.038	-.067	-.088	-.095	-.089	-.086	-.083	-.080	-.077	-.075	-.072	-.069	-.070	-.068	-.070	-.076	-.084	-.089	-.099	-.095	-.075
2.95	.041	.034	.017	-.009	-.041	-.072	-.099	-.116	-.117	-.107	-.102	-.096	-.090	-.086	-.085	-.082	-.077	-.076	-.074	-.077	-.086	-.094	-.102	-.122	-.122	-.107
4.06	.030	.022	.003	-.026	-.060	-.092	-.118	-.128	-.114	-.069	-.061	-.055	-.048	-.043	-.040	-.036	-.029	-.026	-.023	-.030	-.044	-.051	-.062	-.116	-.135	-.127
4.50	.028	.022	.002	-.029	-.064	-.096	-.121	-.127	-.097	-.052	-.046	-.042	-.037	-.032	-.029	-.026	-.019	-.015	-.013	-.018	-.034	-.038	-.046	-.092	-.130	-.131
4.95	.027	.020	-.001	-.034	-.068	-.104	-.128	-.127	-.076	-.043	-.039	-.037	-.035	-.031	-.029	-.025	-.016	-.011	-.009	-.009	-.020	-.024	-.030	-.070	-.122	-.126
5.39	.023	.016	-.005	-.033	-.068	-.104	-.127	-.117	-.064	-.036	-.032	-.030	-.028	-.026	-.023	-.017	-.007	-.002	-.001	-.010	-.031	-.034	-.036	-.065	-.122	-.138
5.84	.028	.020	-.005	-.037	-.072	-.106	-.123	-.106	-.050	-.029	-.026	-.025	-.024	-.026	-.026	-.021	-.013	-.008	-.007	-.013	-.030	-.030	-.030	-.048	-.103	-.127
6.28	.020	.016	-.002	-.036	-.077	-.111	-.118	-.093	-.044	-.031	-.029	-.030	-.029	-.031	-.031	-.024	-.012	-.004	-.002	-.008	-.028	-.029	-.029	-.042	-.085	-.118
6.72	.022	.014	-.007	-.042	-.080	-.111	-.108	-.078	-.040	-.029	-.028	-.030	-.031	-.036	-.036	-.028	-.016	-.008	-.006	-.012	-.035	-.034	-.032	-.043	-.076	-.111
7.17	.022	.013	-.010	-.044	-.079	-.101	-.097	-.066	-.035	-.026	-.025	-.027	-.030	-.036	-.036	-.029	-.018	-.012	-.010	-.015	-.032	-.030	-.026	-.031	-.053	-.095
7.61	.019	.011	-.010	-.044	-.077	-.091	-.089	-.059	-.034	-.027	-.027	-.030	-.039	-.039	-.039	-.030	-.018	-.010	-.008	-.017	-.036	-.028	-.022	-.027	-.045	-.082
8.06	.030	.018	-.003	-.035	-.066	-.082	-.083	-.051	-.028	-.023	-.022	-.024	-.027	-.035	-.037	-.029	-.017	-.007	-.003	-.012	-.036	-.031	-.024	-.026	-.041	-.078
8.50	.034	.025	.003	-.029	-.058	-.079	-.079	-.047	-.026	-.021	-.021	-.024	-.028	-.036	-.041	-.036	-.026	-.016	-.012	-.021	-.041	-.034	-.027	-.027	-.041	-.076
8.95	.036	.027	.007	-.023	-.052	-.073	-.072	-.037	-.019	-.016	-.017	-.020	-.023	-.031	-.037	-.033	-.022	-.012	-.010	-.020	-.040	-.029	-.024	-.021	-.033	-.068
9.39	.037	.027	.010	-.018	-.049	-.071	-.070	-.036	-.018	-.016	-.017	-.019	-.020	-.027	-.034	-.031	-.022	-.012	-.010	-.018	-.034	-.022	-.019	-.018	-.030	-.063
9.83	.045	.034	.013	-.019	-.050	-.070	-.067	-.035	-.018	-.015	-.016	-.018	-.018	-.024	-.031	-.029	-.019	-.009	-.006	-.016	-.029	-.018	-.016	-.016	-.030	-.062

NACA

TABLE I.- EXPERIMENTAL PRESSURE COEFFICIENTS FOR MODEL AT VARIOUS ANGLES OF ATTACK AND REYNOLDS NUMBERS; $M_o = 1.98$ - Continued

(d) $\alpha=10^{o}$, $Re=0.13\times10^{6}$ per inch

$\frac{x}{d}$	Radial angle, θ, deg															
	0	15	30	45	60	75	90	105	120	135	140	145	150	155	160	165
0.22	0.472	0.465	0.426	0.384	0.331	0.274	0.218	0.177	0.147	0.131	0.127	0.124	0.125	0.121	0.122	0.120
.56	.393	.388	.353	.313	.268	.214	.163	.126	.101	.085	.081	.077	.080	.076	.076	.076
.89	.322	.318	.289	.253	.207	.163	.113	.077	.054	.042	.038	.036	.037	.035	.035	.034
1.22	.272	.270	.241	.206	.163	.120	.072	.041	.019	.008	.005	.004	.006	.005	.008	.008
1.61	.208	.206	.180	.148	.108	.071	.026	-.003	-.019	-.026	-.025	-.028	-.022	-.024	-.024	-.023
2.06	.138	.135	.110	.079	.051	.014	-.024	-.047	-.061	-.066	-.063	-.062	-.059	-.058	-.056	-.055
2.50	.074	.082	.052	.027	-.004	-.031	-.064	-.082	-.088	-.088	-.086	-.085	-.080	-.078	-.076	-.075
2.95	.025	.027	.005	-.020	-.046	-.071	-.101	-.115	-.116	-.110	-.107	-.105	-.100	-.099	-.098	-.095
3.62	.032	.029	.008	-.019	-.044	-.071	-.089	-.083	-.079	-.080	-.079	-.080	-.077	-.075	-.069	-.058
4.06	.030	.016	-.009	-.031	-.056	-.081	-.099	-.094	-.090	-.090	-.093	-.094	-.094	-.086	-.065	-.044
4.50	.018	.016	-.005	-.031	-.060	-.086	-.100	-.090	-.086	-.082	-.091	-.091	-.095	-.078	-.047	-.024
4.95	.023	.018	-.006	-.033	-.060	-.081	-.093	-.086	-.082	-.079	-.083	-.084	-.092	-.066	-.030	-.016
5.39	.020	.013	-.006	-.029	-.059	-.081	-.089	-.083	-.084	-.085	-.084	-.083	-.085	-.061	-.031	-.019
5.84	.029	.025	.000	-.033	-.062	-.082	-.085	-.079	-.077	-.085	-.088	-.089	-.087	-.062	-.035	-.020
6.28	.032	.029	.002	-.029	-.059	-.074	-.074	-.070	-.072	-.086	-.087	-.093	-.091	-.060	-.033	-.019
6.72	.030	.026	.003	-.022	-.049	-.064	-.063	-.058	-.060	-.070	-.074	-.075	-.075	-.050	-.022	-.012
7.17	.036	.030	.005	-.022	-.048	-.061	-.058	-.055	-.058	-.064	-.069	-.074	-.072	-.051	-.029	-.014
7.61	.032	.025	.002	-.026	-.053	-.063	-.064	-.060	-.058	-.070	-.072	-.074	-.075	-.056	-.034	-.019
8.06	.036	.030	.007	-.023	-.049	-.059	-.053	-.053	-.053	-.060	-.063	-.067	-.068	-.057	-.036	-.020
8.50	.055	.050	.025	-.004	-.026	-.033	-.031	-.028	-.030	-.036	-.038	-.041	-.041	-.036	-.024	-.008
8.95	.040	.032	.010	- 017	-.044	-.050	-.048	-.043	-.045	-.051	-.053	-.055	-.056	-.062	-.039	-.028
9.39	.041	.034	.012	-.016	-.039	-.042	-.042	-.042	-.039	-.043	-.048	-.049	-.047	-.047	-.038	-.025
9.83	.041	.030	.008	-.019	-.041	-.043	-.039	-.037	-.038	-.044	-.046	-.047	-.046	-.047	-.039	-.030

$\frac{x}{d}$	Radial angle, θ, deg																		
	170	175	180	185	190	195	200	210	215	220	225	240	255	270	285	300	315	330	345
0.22	0.117	0.119	0.120	0.115	0.118	0.120	0.120	0.125	0.123	0.126	0.135	0.156	0.184	0.232	0.285	0.339	0.389	0.429	0.452
.56	.074	.073	.074	.072	.072	.074	.073	.076	.074	.080	.084	.099	.127	.166	.215	.266	.312	.353	.374
.89	.036	.035	.037	.035	.036	.037	.037	.035	.035	.036	.040	.054	.074	.112	.156	.204	.243	.286	.310
1.22	.007	.006	.005	.008	.007	.008	.006	.005	.003	.004	.009	.018	.038	.072	.113	.157	.197	.239	.261
1.61	-.021	-.023	-.024	-.020	-.021	-.021	-.021	-.029	-.029	-.028	-.027	-.022	-.009	.025	.060	.101	.140	.179	.200
2.06	-.053	-.053	-.051	-.050	-.049	-.051	-.054	-.055	-.061	-.059	-.062	-.060	-.055	-.020	.006	.043	.075	.116	.135
2.50	-.074	-.074	-.072	-.069	-.069	-.072	-.073	-.077	-.081	-.078	-.084	-.090	-.086	-.063	-.038	-.005	.022	.059	.074
2.95	-.094	-.090	-.089	-.088	-.088	-.092	-.095	-.099	-.101	-.099	-.107	-.113	-.118	-.102	-.080	-.046	-.022	.012	.027
3.62	-.047	-.044	-.041	-.042	-.049	-.060	-.069	-.076	-.076	-.074	-.077	-.078	-.083	-.083	-.069	-.039	-.013	.021	.039
4.06	-.038	-.036	-.035	-.037	-.045	-.055	-.077	-.094	-.094	-.086	-.093	-.094	-.096	-.101	-.091	-.058	-.030	.006	.022
4.50	-.022	-.022	-.022	-.025	-.028	-.038	-.060	-.091	-.086	-.078	-.081	-.086	-.085	-.092	-.089	-.060	-.033	.003	.019
4.95	-.013	-.012	-.009	-.011	-.017	-.020	-.039	-.075	-.071	-.062	-.072	-.078	-.079	-.082	-.073	-.049	-.028	.008	.025
5.39	-.014	-.012	-.009	-.016	-.020	-.024	-.039	-.072	-.068	-.063	-.075	-.075	-.077	-.082	-.078	-.050	-.018	.018	.032
5.84	-.014	-.013	-.010	-.013	-.018	-.024	-.045	-.079	-.077	-.069	-.077	-.069	-.072	-.074	-.081	-.054	-.026	.015	.033
6.28	-.013	-.013	-.011	-.010	-.013	-.019	-.042	-.080	-.078	-.066	-.078	-.068	-.066	-.069	-.073	-.054	-.030	.011	.027
6.72	-.007	-.005	-.003	-.004	-.008	-.014	-.032	-.064	-.060	-.055	-.061	-.053	-.046	-.052	-.058	-.044	-.017	.020	.035
7.17	-.009	-.007	-.005	-.007	-.013	-.018	-.036	-.061	-.058	-.051	-.057	-.049	-.047	-.049	-.054	-.039	-.017	.019	.037
7.61	-.013	-.009	-.009	-.011	-.018	-.026	-.045	-.067	-.066	-.057	-.061	-.054	-.051	-.052	-.059	-.042	-.019	.017	.033
8.06	-.016	-.013	-.011	-.016	-.022	-.030	-.045	-.061	-.058	-.052	-.053	-.046	-.045	-.044	-.050	-.040	-.017	.020	.035
8.50	-.001	.003	.002	.000	-.006	-.014	-.027	-.033	-.035	-.030	-.030	-.022	-.025	-.019	-.029	-.016	.005	.039	.055
8.95	-.020	-.016	-.013	-.017	-.024	-.032	-.044	-.049	-.049	-.043	-.043	-.036	-.037	-.037	-.043	-.035	-.011	.027	.041
9.39	-.018	-.014	-.013	-.014	-.020	-.027	-.035	-.038	-.039	-.035	-.035	-.028	-.029	-.028	-.036	-.022	-.005	.027	.044
9.83	-.022	-.019	-.017	-.018	-.025	-.031	-.036	-.038	-.039	-.036	-.035	-.030	-.031	-.033	-.039	-.028	-.009	.025	.039

(e) $\alpha=15^{o}$, $Re=0.39\times10^{6}$ per inch

$\frac{x}{d}$	Radial angle, θ, deg															
	0	15	30	45	60	75	90	105	120	135	140	145	150	155	160	165
0.22	0.597	0.576	0.518	0.422	0.332	0.238	0.153	0.090	0.053	0.043	0.043	0.046	0.049	0.054	0.057	0.058
.56	.524	.492	.453	.383	.297	.206	.125	.062	.024	.015	.016	.019	.021	.025	.028	.028
.89	.441	.433	.390	.321	.241	.154	.076	.017	-.018	-.019	-.018	-.013	-.010	-.006	-.004	-.003
1.22	.400	.380	.337	.270	.191	.108	.034	-.021	-.051	-.048	-.045	-.041	-.037	-.033	-.032	-.032
1.61	.326	.310	.270	.208	.136	.060	-.008	-.057	-.084	-.076	-.073	-.068	-.065	-.063	-.060	-.061
2.06	.245	.230	.196	.140	.073	.002	-.062	-.108	-.125	-.115	-.109	-.101	-.095	-.088	-.089	-.076
2.50	.170	.158	.124	.073	.012	-.053	-.111	-.151	-.164	-.150	-.141	-.123	-.113	-.104	-.095	-.092
2.95	.116	.106	.075	.027	-.031	-.091	-.143	-.179	-.187	-.171	-.162	-.139	-.118	-.104	-.097	-.095
3.62	.100	.086	.052	.002	-.058	-.121	-.174	-.196	-.185	-.179	-.166	-.124	-.094	-.085	-.076	-.071
4.06	.098	.082	.046	-.006	-.068	-.130	-.186	-.183	-.180	-.175	-.177	-.148	-.102	-.074	-.060	-.058
4.50	.093	.078	.043	-.011	-.072	-.137	-.186	-.177	-.156	-.180	-.184	-.172	-.129	-.076	-.054	-.048
4.95	.089	.074	.038	-.018	-.081	-.142	-.185	-.166	-.131	-.176	-.188	-.191	-.162	-.101	-.063	-.053
5.39	.088	.073	.038	-.018	-.082	-.149	-.185	-.151	-.128	-.168	-.185	-.203	-.185	-.126	-.074	-.055
5.84	.092	.080	.038	-.021	-.086	-.151	-.172	-.120	-.111	-.157	-.174	-.193	-.193	-.145	-.094	-.071
6.28	.080	.067	.033	-.023	-.090	-.142	-.150	-.121	-.101	-.150	-.162	-.175	-.187	-.152	-.105	-.076
6.72	.083	.067	.027	-.031	-.098	-.139	-.134	-.108	-.095	-.126	-.137	-.148	-.167	-.151	-.118	-.086
7.17	.081	.065	.025	-.034	-.101	-.146	-.123	-.093	-.090	-.097	-.105	-.108	-.129	-.126	-.119	-.097
7.61	.077	.061	.023	-.036	-.104	-.150	-.115	-.087	-.096	-.084	-.087	-.085	-.097	-.096	-.107	-.098
8.06	.088	.069	.029	-.030	-.100	-.150	-.108	-.078	-.096	-.079	-.076	-.074	-.076	-.084	-.103	-.097
8.50	.092	.075	.032	-.029	-.099	-.148	-.099	-.068	-.082	-.076	-.073	-.071	-.070	-.085	-.099	-.095
8.95	.090	.076	.033	-.028	-.098	-.148	-.082	-.060	-.061	-.067	-.065	-.065	-.065	-.078	-.087	-.082
9.39	.088	.071	.031	-.024	-.094	-.148	-.080	-.055	-.050	-.057	-.057	-.056	-.058	-.063	-.070	-.068
9.83	.090	.074	.031	-.025	-.095	-.146	-.084	-.056	-.049	-.054	-.052	-.052	-.053	-.054	-.059	-.058

$\frac{x}{d}$	Radial angle, θ, deg														
	170	175	180	190	200	210	220	240	255	270	285	300	315	330	345
0.22	0.059	0.058	0.058	0.059	0.054	0.047	0.045	0.058	0.102	0.177	0.259	0.351	0.455	0.531	0.578
.56	.029	.024	.025	.029	.026	.019	.011	.020	.060	.121	.183	.273	.359	.433	.485
.89	-.003	-.003	-.001	-.003	-.005	-.010	-.016	-.022	.003	.060	.137	.223	.305	.376	.425
1.22	-.026	-.019	-.018	-.021	-.032	-.036	-.041	-.052	-.030	.023	.096	.179	.259	.327	.374
1.61	-.043	-.039	-.038	-.039	-.062	-.067	-.069	-.084	-.073	-.025	.044	.121	.195	.258	.304
2.06	-.059	-.058	-.057	-.058	-.095	-.101	-.104	-.124	-.120	-.076	-.014	.056	.124	.183	.223
2.50	-.082	-.079	-.076	-.077	-.095	-.124	-.133	-.155	-.162	-.124	-.068	-.003	.059	.113	.151
2.95	-.089	-.083	-.079	-.083	-.104	-.120	-.138	-.171	-.191	-.160	-.105	-.045	.012	.063	.099
3.62	-.060	-.050	-.046	-.056	-.081	-.090	-.122	-.178	-.188	-.178	-.123	-.062	-.003	.048	.083
4.06	-.047	-.033	-.031	-.045	-.077	-.104	-.168	-.173	-.176	-.189	-.135	-.090	-.010	.043	.079
4.50	-.040	-.025	-.020	-.036	-.076	-.120	-.178	-.157	-.158	-.171	-.139	-.075	-.014	.039	.076
4.95	-.042	-.020	-.007	-.017	-.069	-.140	-.188	-.136	-.145	-.155	-.135	-.067	-.022	.031	.069
5.39	-.032	-.013	-.006	-.027	-.098	-.182	-.191	-.124	-.140	-.148	-.155	-.086	-.015	.048	.081
5.84	-.037	-.022	-.016	-.026	-.099	-.193	-.179	-.107	-.125	-.133	-.151	-.096	-.033	.026	.069
6.28	-.037	-.024	-.024	-.035	-.099	-.183	-.159	-.105	-.103	-.119	-.135	-.097	-.032	.025	.061
6.72	-.053	-.040	-.040	-.055	-.107	-.165	-.141	-.104	-.102	-.113	-.120	-.098	-.033	.025	.062
7.17	-.070	-.059	-.058	-.072	-.115	-.146	-.120	-.092	-.096	-.103	-.109	-.106	-.038	.023	.064
7.61	-.076	-.066	-.065	-.079	-.114	-.112	-.099	-.082	-.085	-.096	-.102	-.098	-.034	.020	.059
8.06	-.078	-.069	-.066	-.075	-.092	-.088	-.085	-.079	-.081	-.086	-.102	-.092	-.033	.026	.068
8.50	-.076	-.070	-.068	-.078	-.088	-.082	-.079	-.078	-.071	-.096	-.111	-.093	-.033	.030	.076
8.95	-.067	-.065	-.068	-.074	-.076	-.069	-.067	-.061	-.054	-.101	-.118	-.087	-.029	.028	.072
9.39	-.061	-.061	-.062	-.065	-.064	-.055	-.054	-.049	-.048	-.109	-.123	-.088	-.029	.028	.072
9.83	-.053	-.052	-.052	-.053	-.051	-.044	-.043	-.043	-.049	-.116	-.126	-.087	-.026	.030	.072

NACA

TABLE I.- EXPERIMENTAL PRESSURE COEFFICIENTS FOR MODEL AT VARIOUS ANGLES OF ATTACK AND REYNOLDS NUMBERS; M_0 = 1.98 - Continued

(f) $\alpha=15^{\circ}$, Re=0.39×10^{6} per inch with tunnel turbulence grid

$\frac{x}{d}$	Radial angle, θ, deg																												
	0	15	30	45	60	75	90	105	120	135	140	145	150	155	160	165	170	175	180	185	190	195	200	210	215	220	225	240	255	270
0.22	0.600	0.579	0.520	0.467	0.362	0.264	0.177	0.110	0.077	0.064	0.063	0.065	0.066	0.067	0.069	0.071	0.070	0.073	0.071	0.071	0.066	0.068	0.065	0.062	0.061	0.062	0.064	0.084	0.134	0.207
.56	.522	.506	.456	.382	.297	.206	.125	.063	.029	.022	.024	.026	.028	.030	.032	.033	.034	.035	.034	.034	.032	.031	.028	.022	.021	.018	-.017	0.029	0.068	0.132
.89	.437	.426	.381	.313	.233	.150	.075	.017	-.012	-.015	-.014	-.009	-.006	-.003	-.001	.000	.001	.003	.002	.002	.000	-.002	-.003	-.009	-.012	-.017	-.019	-.017	.015	.071
1.22	.394	.374	.330	.263	.186	.107	.036	-.019	-.045	-.044	-.042	-.037	-.034	-.031	-.028	-.025	-.020	-.015	-.015	-.017	-.022	-.027	-.029	-.037	-.040	-.044	-.048	-.048	-.020	.033
1.61	.324	.306	.265	.203	.130	.057	-.011	-.061	-.081	-.079	-.075	-.068	-.061	-.057	-.053	-.048	-.039	-.037	-.035	-.036	-.038	-.047	-.052	-.063	-.069	-.077	-.082	-.087	-.064	-.017
2.06	.244	.228	.190	.135	.066	.000	-.062	-.108	-.124	-.115	-.108	-.095	-.083	-.078	-.073	-.067	-.061	-.057	-.057	-.059	-.061	-.068	-.072	-.085	-.096	-.108	-.117	-.128	-.111	-.069
2.50	.169	.155	.121	.069	.007	-.053	-.109	-.148	-.163	-.143	-.130	-.113	-.101	-.096	-.090	-.086	-.080	-.077	-.076	-.077	-.081	-.086	-.089	-.102	-.114	-.129	-.144	-.166	-.154	-.118
2.95	.115	.103	.071	.021	-.037	-.093	-.146	-.185	-.188	-.161	-.146	-.123	-.108	-.102	-.096	-.093	-.087	-.082	-.081	-.083	-.087	-.092	-.096	-.109	-.122	-.141	-.160	-.190	-.188	-.153
3.62	.100	.085	.051	-.001	-.060	-.117	-.170	-.197	-.185	-.158	-.133	-.102	-.086	-.079	-.073	-.066	-.057	-.048	-.046	-.052	-.062	-.072	-.078	-.095	-.108	-.137	-.159	-.191	-.197	-.172
4.06	.097	.082	.046	-.007	-.069	-.129	-.182	-.190	-.178	-.158	-.141	-.111	-.090	-.078	-.070	-.061	-.046	-.034	-.033	-.042	-.056	-.069	-.077	-.097	-.114	-.141	-.161	-.185	-.192	-.185
4.50	.094	.079	.043	-.013	-.076	-.136	-.183	-.176	-.163	-.159	-.155	-.134	-.107	-.088	-.072	-.056	-.038	-.024	-.022	-.032	-.050	-.066	-.079	-.112	-.132	-.145	-.153	-.167	-.180	-.187
4.95	.094	.079	.041	-.016	-.081	-.144	-.170	-.159	-.144	-.156	-.164	-.154	-.130	-.104	-.080	-.057	-.034	-.016	-.013	-.023	-.042	-.064	-.084	-.130	-.148	-.153	-.151	-.143	-.161	-.171
5.39	.091	.076	.037	-.018	-.084	-.145	-.153	-.134	-.125	-.150	-.164	-.165	-.146	-.118	-.082	-.049	-.023	-.005	-.002	-.015	-.040	-.070	-.103	-.159	-.171	-.166	-.155	-.131	-.149	-.169
5.84	.092	.075	.038	-.019	-.086	-.145	-.142	-.109	-.108	-.141	-.159	-.171	-.167	-.137	-.093	-.054	-.026	-.010	-.005	-.015	-.038	-.072	-.112	-.176	-.176	-.163	-.144	-.112	-.125	-.158
6.28	.091	.077	.037	-.023	-.092	-.139	-.130	-.100	-.099	-.134	-.150	-.166	-.172	-.140	-.093	-.054	-.029	-.016	-.011	-.021	-.040	-.071	-.117	-.175	-.163	-.148	-.133	-.099	-.110	-.143
6.72	.090	.075	.034	-.025	-.092	-.129	-.118	-.095	-.091	-.116	-.125	-.141	-.157	-.141	-.097	-.060	-.039	-.027	-.025	-.033	-.047	-.075	-.117	-.154	-.137	-.125	-.120	-.091	-.096	-.128
7.17	.095	.076	.033	-.027	-.096	-.121	-.109	-.092	-.086	-.097	-.098	-.109	-.129	-.130	-.103	-.074	-.054	-.043	-.042	-.048	-.059	-.084	-.113	-.127	-.108	-.099	-.098	-.083	-.083	-.117
7.61	.094	.076	.033	-.031	---	-.115	-.102	-.087	-.085	-.081	-.079	-.086	-.102	-.111	-.098	-.077	-.063	-.053	-.054	-.061	-.071	-.092	-.107	-.098	-.081	-.078	-.080	-.075	-.070	-.107
8.06	.100	.082	.039	-.025	-.094	-.115	-.097	-.079	-.078	-.070	-.069	-.070	-.079	-.089	-.086	-.074	-.064	-.056	-.055	-.060	-.069	-.084	-.090	-.075	-.065	-.066	-.071	-.074	-.064	-.096
8.50	.100	.083	.038	-.025	-.092	-.113	-.093	-.065	-.066	-.061	-.060	-.059	-.065	-.075	-.076	-.071	-.063	-.057	-.055	-.061	-.069	-.081	-.081	-.061	-.055	-.056	-.062	-.067	-.061	-.092
8.95	.099	.082	.037	-.027	-.094	-.117	-.090	-.059	-.056	-.055	-.054	-.052	-.057	-.062	-.066	-.064	-.059	-.054	-.054	-.057	-.064	-.069	-.068	-.054	-.049	-.049	-.052	-.055	-.058	-.091
9.39	.096	.079	.035	-.027	-.094	-.117	-.090	-.056	-.048	-.051	-.049	-.048	-.051	-.057	-.057	-.057	-.052	-.048	-.048	-.050	-.053	-.056	-.055	-.047	-.046	-.044	-.045	-.049	-.055	-.088
9.83	.091	.079	.032	-.031	-.096	-.119	-.094	-.055	-.048	-.046	-.046	-.045	-.048	-.051	-.052	-.052	-.047	-.043	-.044	-.044	-.046	-.048	-.046	-.041	-.041	-.041	-.040	-.045	-.054	-.094

(g) $\alpha=15^{\circ}$, Re=0.13×10^{6} per inch

$\frac{x}{d}$	Radial angle, θ, deg																									
	0	15	30	45	60	75	90	105	120	135	140	145	150	155	160	165	170	175	180	190	200	210	220	240	255	270
0.22	0.603	0.584	0.532	0.452	0.357	0.263	0.185	0.112	0.071	0.056	0.053	0.052	0.055	0.057	0.057	0.061	0.059	0.061	0.059	0.061	0.055	0.053	0.051	0.068	0.112	0.182
.56	.526	.511	.463	.389	.302	.209	.137	.064	.026	.016	.013	.012	.016	.018	.021	.022	.020	.024	.024	.023	.018	.015	.008	.015	.051	.114
.89	.445	.436	.391	.323	.243	.156	.086	.019	-.014	-.021	-.020	-.020	-.016	-.013	-.011	-.008	-.009	-.005	-.005	-.007	-.012	-.015	-.023	-.026	.000	.053
1.22	.382	.371	.331	.267	.191	.111	.046	-.018	-.048	-.050	-.049	-.046	-.042	-.039	-.037	-.034	-.034	-.030	-.026	-.029	-.038	-.042	-.049	-.056	-.038	.021
1.61	.312	.302	.265	.204	.133	.057	-.004	-.061	-.087	-.079	-.078	-.076	-.071	-.070	-.066	-.063	-.061	-.055	-.049	-.051	-.068	-.070	-.076	-.089	-.081	-.039
2.06	.240	.220	.188	.129	.066	-.003	-.058	-.109	-.123	-.112	-.108	-.109	-.105	-.104	-.107	-.099	-.086	-.078	-.072	-.071	-.103	-.120	-.099	-.110	-.115	-.093
2.50	.152	.144	.115	.065	.005	-.056	-.105	-.147	-.153	-.140	-.139	-.138	-.136	-.137	-.136	-.124	-.098	-.090	-.087	-.088	-.127	-.134	-.138	-.143	-.157	-.137
2.95	.102	.095	.068	.020	-.036	-.096	-.135	-.170	-.162	-.154	-.153	-.155	-.155	-.162	-.163	-.122	-.096	-.090	-.088	-.088	-.134	-.159	-.159	-.163	-.174	-.165
4.06	.081	.070	.039	-.012	-.073	-.128	-.154	-.154	-.152	-.149	-.161	-.173	-.182	-.186	-.113	-.061	-.051	-.047	-.045	-.047	-.093	-.132	-.145	-.156	-.156	-.170
4.50	.089	.079	.050	.003	-.052	-.106	-.122	-.119	-.125	-.117	-.134	-.136	-.137	-.141	-.080	-.038	-.025	-.022	-.020	-.025	-.068	-.136	-.135	-.126	-.121	-.123
4.95	.077	.069	.040	-.011	-.074	-.133	-.141	-.141	-.144	-.137	-.143	-.142	-.142	-.149	-.112	-.072	-.053	-.044	-.037	-.042	-.092	-.139	-.143	-.143	-.136	-.142
5.39	.083	.072	.039	-.018	-.082	-.135	-.136	-.136	-.134	-.134	-.139	-.141	-.140	-.146	-.127	-.095	-.076	-.066	-.059	-.065	-.112	-.142	-.142	-.131	-.127	-.128
5.84	.080	.073	.038	-.021	-.088	-.132	-.124	-.122	-.125	-.138	-.141	-.142	-.142	-.148	-.131	-.101	-.085	-.075	-.066	-.071	-.117	-.138	-.137	-.125	-.118	-.118
6.28	.075	.066	.028	-.029	-.093	-.123	-.114	-.115	-.117	-.135	-.137	-.139	-.138	-.145	-.133	-.106	-.085	-.075	-.066	-.075	-.120	-.137	-.135	-.118	-.113	-.112
6.72	.071	.062	.024	-.035	-.100	-.115	-.107	-.106	-.109	-.129	-.131	-.132	-.132	-.140	-.135	-.115	-.095	-.084	-.073	-.085	-.128	-.132	-.130	-.111	-.106	-.106
7.17	.072	.063	.024	-.035	-.095	-.103	-.096	-.098	-.099	-.120	-.125	-.124	-.125	-.126	-.126	-.114	-.098	-.089	-.078	-.086	-.117	-.118	-.120	-.099	-.098	-.096
7.61	.071	.062	.024	-.035	-.090	-.097	-.092	-.093	-.097	-.112	-.115	-.114	-.114	-.117	-.119	-.108	-.096	-.087	-.078	-.084	-.110	-.108	-.109	-.097	-.092	-.088
8.06	.086	.076	.034	-.026	-.077	-.086	-.080	-.080	-.081	-.094	-.095	-.096	-.096	-.098	-.100	-.093	-.085	-.078	-.069	-.073	-.095	-.093	-.092	-.083	-.079	-.076
8.50	.083	.071	.029	-.028	-.078	-.094	-.085	-.086	-.085	-.094	-.095	-.095	-.093	-.096	-.097	-.093	-.087	-.083	-.076	-.080	-.095	-.092	-.092	-.086	-.082	-.082
8.95	.084	.075	.032	-.022	-.078	-.090	-.083	-.082	-.082	-.086	-.087	-.088	-.086	-.087	-.086	-.084	-.079	-.075	-.070	-.073	-.086	-.085	-.085	-.080	-.079	-.079
9.39	.088	.075	.033	-.022	-.077	-.089	-.082	-.074	-.079	-.081	-.082	-.082	-.081	-.082	-.081	-.078	-.074	-.069	-.066	-.069	-.080	-.079	-.079	-.077	-.070	-.073
9.83	.083	.071	.028	-.028	-.081	-.083	-.072	-.058	-.070	-.074	-.078	-.077	-.075	-.078	-.078	-.074	-.071	-.066	-.062	-.066	-.076	-.075	-.076	-.072	-.052	-.062

NACA

TABLE I.- EXPERIMENTAL PRESSURE COEFFICIENTS FOR MODEL AT VARIOUS ANGLES OF ATTACK AND REYNOLDS NUMBERS; M_o = 1.98 - Concluded

(h) $\alpha=20^o$, Re=0.39×10^6 per inch

$\frac{x}{d}$	Radial angle, θ, deg																									
	0	15	30	45	60	75	90	105	120	135	140	145	150	155	160	165	170	175	180	190	200	210	220	240	255	270
0.22	0.768	0.735	0.653	0.537	0.399	0.256	0.126	0.027	-0.021	-0.011	-0.006	-0.005	0.002	0.004	0.004	0.005	0.009	0.018	0.020	0.006	0.004	-0.001	-0.011	-0.017	0.046	0.153
.56	.686	.657	.581	.473	.343	.210	.085	-.013	-.062	-.047	-.042	-.039	-.037	-.036	-.037	-.038	-.009	.004	.003	-.017	-.037	-.039	-.044	-.065	-.013	.086
.89	.597	.571	.502	.401	.280	.154	.037	-.055	-.102	-.081	-.077	-.075	-.074	-.075	-.081	-.080	-.024	-.022	-.022	-.022	-.081	-.075	-.078	-.105	-.066	.024
1.22	.527	.499	.433	.337	.224	.107	-.001	-.088	-.132	-.108	-.101	-.102	-.103	-.102	-.110	-.082	-.038	-.038	-.039	-.039	-.113	-.109	-.105	-.136	-.102	-.017
1.61	.442	.420	.359	.272	.166	.057	-.044	-.126	-.165	-.138	-.136	-.137	-.138	-.128	-.126	-.094	-.057	-.056	-.057	-.056	-.128	-.132	-.133	-.164	-.141	-.066
2.06	.350	.330	.275	.192	.095	-.006	-.096	-.170	-.187	-.178	-.175	-.176	-.176	---	-.155	-.122	-.087	-.081	-.078	-.085	-.147	-.169	-.174	-.184	-.183	-.116
2.50	.267	.249	.197	.122	.033	-.056	-.138	-.204	-.202	-.204	-.203	-.193	-.181	-.186	-.185	-.144	-.107	-.096	-.094	-.100	-.170	-.189	-.202	-.202	-.218	-.160
2.95	.207	.191	.143	.072	-.011	-.095	-.171	-.225	-.207	-.214	-.217	-.228	-.229	-.224	-.209	-.160	-.116	-.099	-.093	-.104	-.185	-.227	-.223	-.212	-.226	-.191
4.06	.179	.157	.104	.031	-.054	-.136	-.202	-.186	-.179	-.203	-.243	-.240	-.245	-.254	-.200	-.145	-.110	-.092	-.089	-.112	-.202	-.243	-.247	-.186	-.189	-.206
4.50	.175	.154	.102	.028	-.058	-.141	-.178	-.165	-.167	-.230	-.224	-.222	-.229	-.238	-.198	-.154	-.123	-.104	-.100	-.126	-.202	-.226	-.227	-.170	-.163	-.166
4.95	.171	.150	.097	.022	-.062	-.144	-.165	-.153	-.163	-.206	-.205	-.204	-.212	-.225	-.206	-.167	-.135	-.112	-.102	-.125	-.197	-.196	-.202	-.157	-.142	-.156
5.39	.183	.149	.096	.020	-.068	-.152	-.155	-.153	-.153	-.188	-.177	-.176	-.183	-.195	-.199	-.169	-.142	-.121	-.115	-.140	-.201	-.183	-.180	-.151	-.160	-.157
5.84	.169	.153	.100	.020	-.069	-.152	-.146	-.145	-.143	-.161	-.151	-.149	-.153	-.159	-.179	-.171	-.150	-.133	-.126	-.147	-.186	-.151	-.148	-.157	-.155	-.148
6.28	.159	.140	.089	.013	-.074	-.158	-.144	-.146	-.141	-.145	-.140	-.136	-.132	-.134	-.151	-.154	-.148	-.137	-.132	-.142	-.141	-.126	-.134	-.149	-.148	-.145
6.72	.159	.137	.081	.005	-.081	-.160	-.146	-.146	-.142	-.136	-.132	-.128	-.124	-.126	-.133	-.136	-.135	-.131	-.131	-.119	-.125	-.125	-.134	-.135	-.142	-.145
7.17	.162	.141	.085	.004	-.083	-.162	-.145	-.138	-.135	-.131	-.129	-.128	-.126	-.129	-.133	-.130	-.118	-.109	-.108	-.114	-.137	-.125	-.135	-.130	-.138	-.139
7.61	.154	.132	.078	.000	-.088	-.158	-.139	-.136	-.133	-.130	-.127	-.125	-.125	-.128	-.131	-.126	-.122	-.115	-.117	-.123	-.126	-.126	-.125	-.133	-.126	-.131
8.06	.166	.140	.084	.005	-.084	-.151	-.135	-.126	-.127	-.126	-.125	-.125	-.127	-.130	-.127	-.122	-.109	-.102	-.100	-.105	-.119	-.120	-.119	-.119	-.109	-.128
8.50	.169	.147	.087	.005	-.083	-.148	-.133	-.118	-.122	-.123	-.124	-.124	-.128	-.132	-.132	-.127	-.115	-.109	-.110	-.115	-.127	-.128	-.119	-.112	-.104	-.131
8.95	.173	.151	.093	.005	-.082	-.150	-.129	-.109	-.111	-.116	-.117	-.120	-.122	-.128	-.129	-.126	-.116	-.108	-.107	-.119	-.127	-.119	-.111	-.104	-.107	-.129
9.39	.168	.146	.089	.005	-.084	-.158	-.128	-.100	-.100	-.106	-.106	-.109	-.111	-.119	-.122	-.121	-.114	-.106	-.103	-.112	-.115	-.103	-.101	-.101	-.099	-.140
9.83	.174	.151	.092	.005	-.086	-.161	-.135	-.098	-.099	-.102	-.101	-.098	-.102	-.106	-.107	-.106	-.102	-.097	-.093	-.099	-.099	-.089	-.097	-.091	-.104	-.144

(i) $\alpha=20^o$, Re=0.39×10^6 with tunnel turbulence grid

$\frac{x}{d}$	Radial angle, θ, deg																												
	0	15	30	60	75	90	105	120	135	140	145	150	155	160	165	170	175	180	185	190	195	200	210	215	220	225	240	255	270
0.22	---	---	---	---	0.245	0.119	0.024	-0.018	-0.009	-0.005	0	0.004	0.005	0.007	0.007	0.014	0.021	0.022	0.015	0.008	0.005	0.004	-0.003	-0.007	-0.013	-0.018	-0.010	0.056	0.170
.56	.664	.639	.563	.321	.191	.073	-.019	-.061	-.046	-.042	-.039	-.037	-.037	-.038	-.037	-.017	-.003	-.001	-.012	-.032	-.039	-.038	-.040	-.044	-.048	-.056	-.064	-.011	.091
.89	.570	.550	.483	.258	.136	.026	-.062	-.100	-.081	-.076	-.076	-.075	-.077	-.078	-.069	-.038	-.027	-.024	-.029	-.042	-.072	-.080	-.076	-.078	-.080	-.087	-.103	-.062	.028
1.22	.520	.490	.424	.210	.098	-.010	-.095	-.128	-.109	-.106	-.106	-.104	-.103	-.101	-.069	-.044	-.040	-.041	-.042	-.047	-.075	-.104	-.103	-.105	-.107	-.114	-.133	-.095	-.009
1.61	.437	.412	.352	.150	.044	-.053	-.134	-.160	-.141	-.136	-.135	-.133	-.133	-.125	-.085	-.062	-.058	-.058	-.059	-.064	-.088	-.116	-.133	-.137	-.141	-.148	-.165	-.136	-.057
2.06	.347	.323	.267	.082	-.016	-.103	-.175	-.189	-.175	-.171	-.167	-.156	-.153	-.146	-.108	-.083	-.079	-.079	-.082	-.089	-.113	-.138	-.160	-.169	-.174	-.180	-.197	-.179	-.105
2.50	.265	.244	.192	.022	-.067	-.145	-.210	-.208	-.204	-.203	-.201	-.189	-.178	-.166	-.132	-.105	-.097	-.097	-.102	-.112	-.136	-.160	-.186	-.201	-.203	-.207	-.212	-.214	-.150
2.95	.204	.185	.137	-.023	-.106	-.179	-.229	-.219	-.221	-.223	-.226	-.218	-.207	-.186	-.149	-.117	-.105	-.104	-.109	-.124	-.153	-.182	-.219	-.228	-.227	-.223	-.221	-.231	-.183
3.62	.182	.160	.107	-.055	-.136	-.204	-.205	-.201	-.213	-.225	-.238	-.243	-.231	-.185	-.131	-.090	-.074	-.072	-.084	-.114	-.161	-.210	-.238	-.231	-.219	-.209	-.203	-.208	-.195
4.06	.178	.153	.100	-.066	-.147	-.204	-.195	-.191	-.213	-.235	-.244	-.250	-.242	-.191	-.134	-.094	-.077	-.076	-.088	-.121	-.173	-.230	-.247	-.239	-.224	-.201	-.195	-.197	-.203
4.50	.175	.152	.096	-.072	-.155	-.184	-.176	-.177	-.228	-.233	-.234	-.237	-.237	-.194	-.144	-.110	-.095	-.093	-.106	-.133	-.175	-.226	-.239	-.237	-.235	-.204	-.175	-.178	-.189
4.95	.172	.149	.094	-.077	-.159	-.167	-.159	-.162	-.215	-.214	-.217	-.221	-.227	-.194	-.155	-.124	-.109	-.106	-.117	-.139	-.174	-.214	-.219	-.217	-.218	-.206	-.156	-.156	-.169
5.39	.175	.148	.091	-.078	-.160	-.156	-.144	-.147	-.189	-.185	-.188	-.193	-.206	-.192	-.159	-.131	-.116	-.114	-.125	-.147	-.178	-.207	-.198	-.195	-.198	-.194	-.148	-.150	-.169
5.84	.175	.153	.096	-.079	-.159	-.151	-.136	-.139	-.165	-.157	-.159	-.162	-.176	-.182	-.163	-.139	-.124	-.121	-.131	-.150	-.175	-.188	-.165	-.161	-.163	-.165	-.142	-.147	-.162
6.28	.170	.147	.091	-.084	-.161	-.150	-.140	-.135	-.142	-.135	-.134	-.137	-.149	-.159	-.153	-.136	-.126	-.124	-.133	-.148	-.159	-.150	-.131	-.132	-.138	-.140	-.143	-.145	-.160
6.72	.171	.146	.090	-.082	-.159	-.148	-.139	-.134	-.125	-.121	-.118	-.117	-.123	-.132	-.132	-.125	-.120	-.121	-.124	-.132	-.131	-.120	-.115	-.115	-.122	-.127	-.134	-.139	-.157
7.17	.177	.153	.093	-.090	-.163	-.151	-.140	-.132	-.124	-.122	-.119	-.115	-.117	-.120	-.117	-.114	-.108	-.108	-.110	-.115	-.118	-.115	-.115	-.115	-.117	-.122	-.127	-.131	-.152
7.61	.173	.157	.085	-.094	-.160	-.147	-.140	-.131	-.122	-.119	-.116	-.115	-.118	-.118	-.113	-.105	-.100	-.101	-.104	-.112	-.117	-.115	-.110	-.111	-.113	-.119	-.126	-.128	-.144
8.06	.183	.147	.096	-.091	-.158	-.141	-.129	-.128	-.118	-.114	-.114	-.113	-.114	-.113	-.108	-.102	-.098	-.096	-.098	-.103	-.107	-.109	-.109	-.110	-.105	-.112	-.121	-.119	-.137
8.50	.184	.159	.096	-.088	-.150	-.132	-.116	-.117	-.116	-.114	-.116	-.115	-.116	-.114	-.108	-.100	-.094	-.094	-.098	-.105	-.111	-.116	-.117	-.118	-.114	-.110	-.110	-.113	-.135
8.95	.183	.157	.095	-.092	-.151	-.127	-.113	-.111	-.111	-.113	-.115	-.116	-.119	-.118	-.112	-.104	-.099	-.100	-.104	-.111	-.116	-.119	-.115	-.117	-.117	-.112	-.107	-.112	-.133
9.39	.179	.155	.092	-.094	-.148	-.123	-.105	-.106	-.107	-.108	-.112	-.114	-.116	-.117	-.114	-.106	-.101	-.101	-.105	-.110	-.114	-.116	-.108	-.108	-.110	-.110	-.105	-.107	-.131
9.83	.177	.152	.089	-.098	-.147	-.122	-.102	-.102	-.104	-.105	-.109	-.109	-.111	-.112	-.109	-.103	-.099	-.098	-.100	-.105	-.107	-.111	-.104	-.104	-.105	-.106	-.100	-.108	-.133

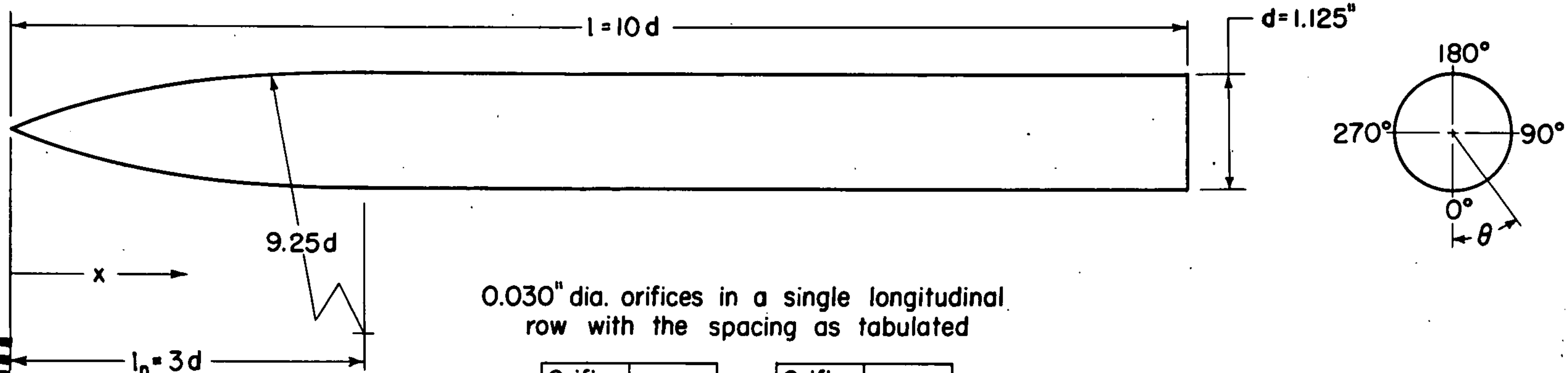

Orifice No.	x/d
1	0.22
2	0.56
3	0.89
4	1.22
5	1.61
6	2.06
7	2.50
8	2.95
9	3.62
10	4.06
11	4.50
12	4.95

Orifice No.	x/d
13	5.39
14	5.84
15	6.28
16	6.72
17	7.17
18	7.61
19	8.06
20	8.50
21	8.95
22	9.39
23	9.83

Figure 1.- Model dimensions and orifice locations.

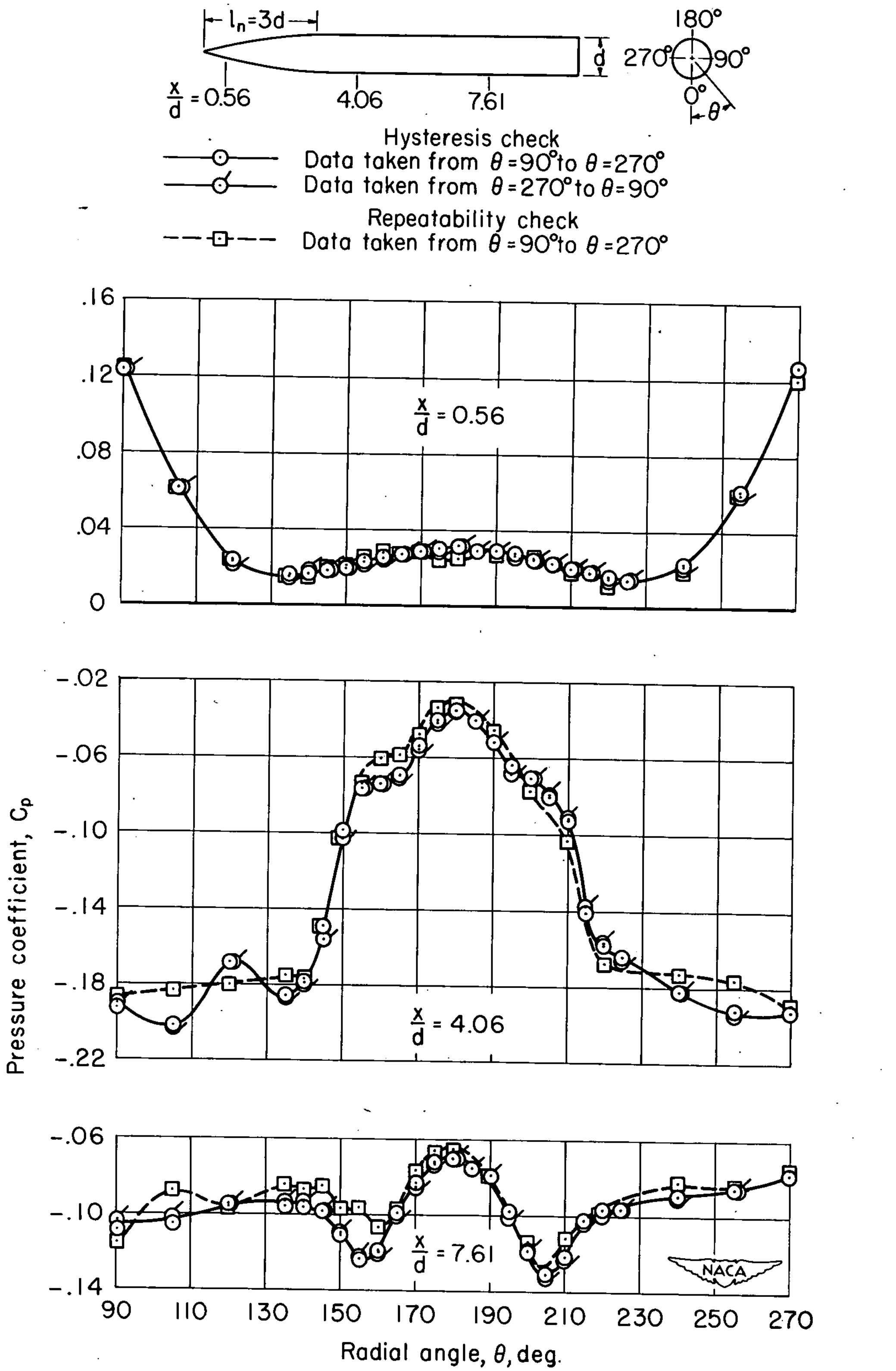

Figure 2.- Circumferential pressure distributions over top half of model; α = 15°, R = 0.39×10^6 per inch, and M_0 = 1.98.

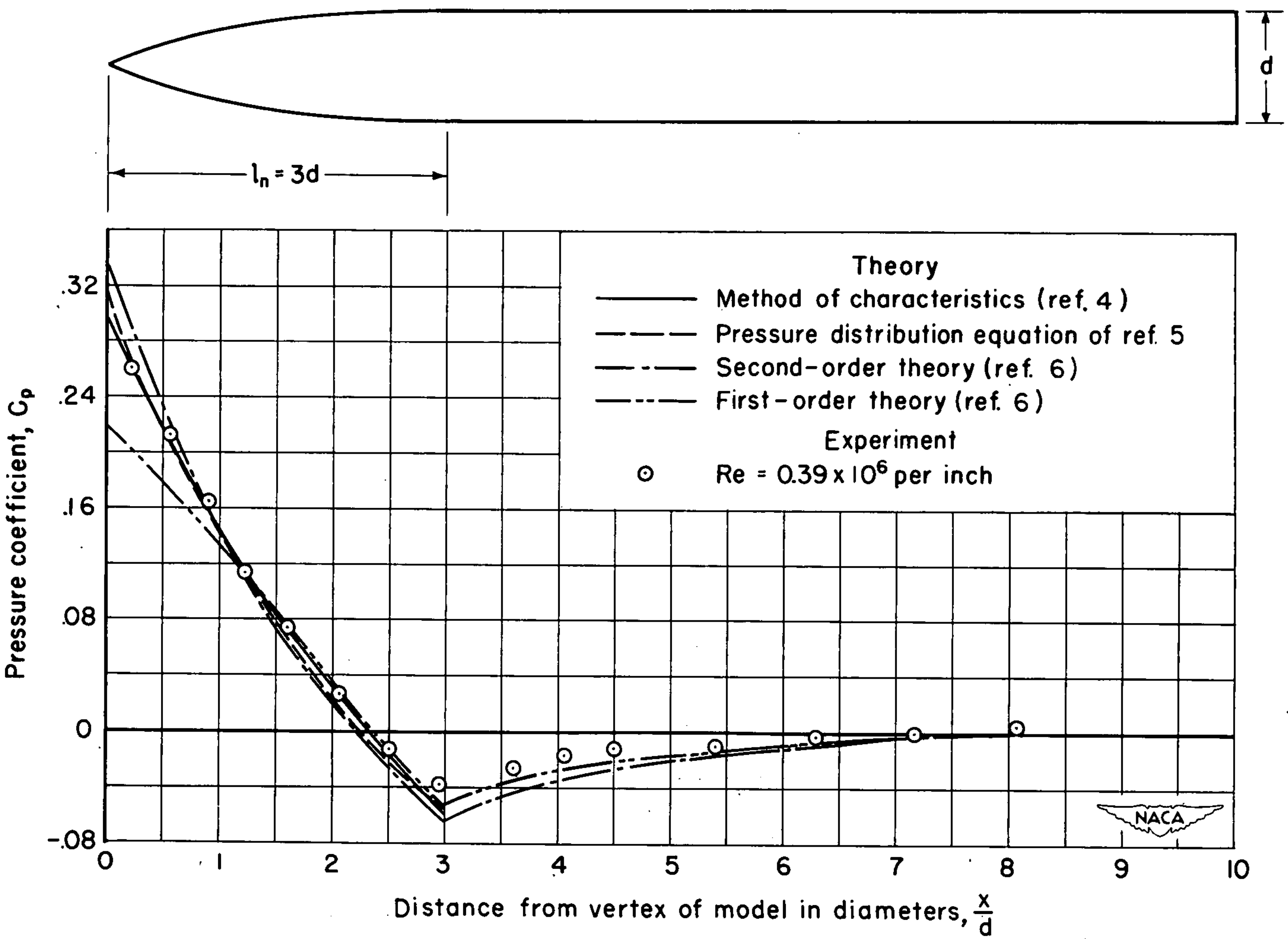

Figure 3.- Comparison of theoretical and experimental longitudinal pressure distributions at zero angle of attack; $M_o = 1.98$.

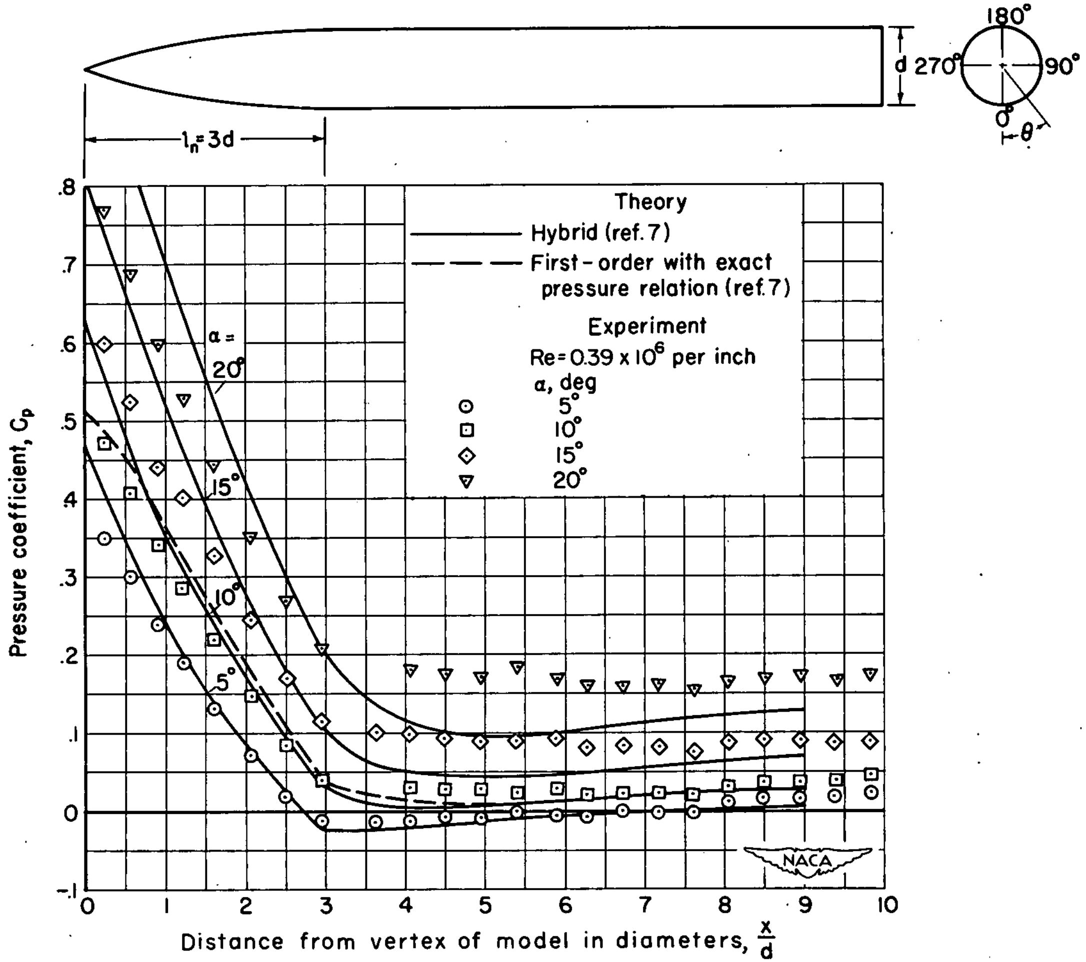

(a) $\theta = 0^{\circ}$

Figure 4.- Comparison of theoretical and experimental longitudinal pressure distributions at various angles of attack; $M_0 = 1.98$.

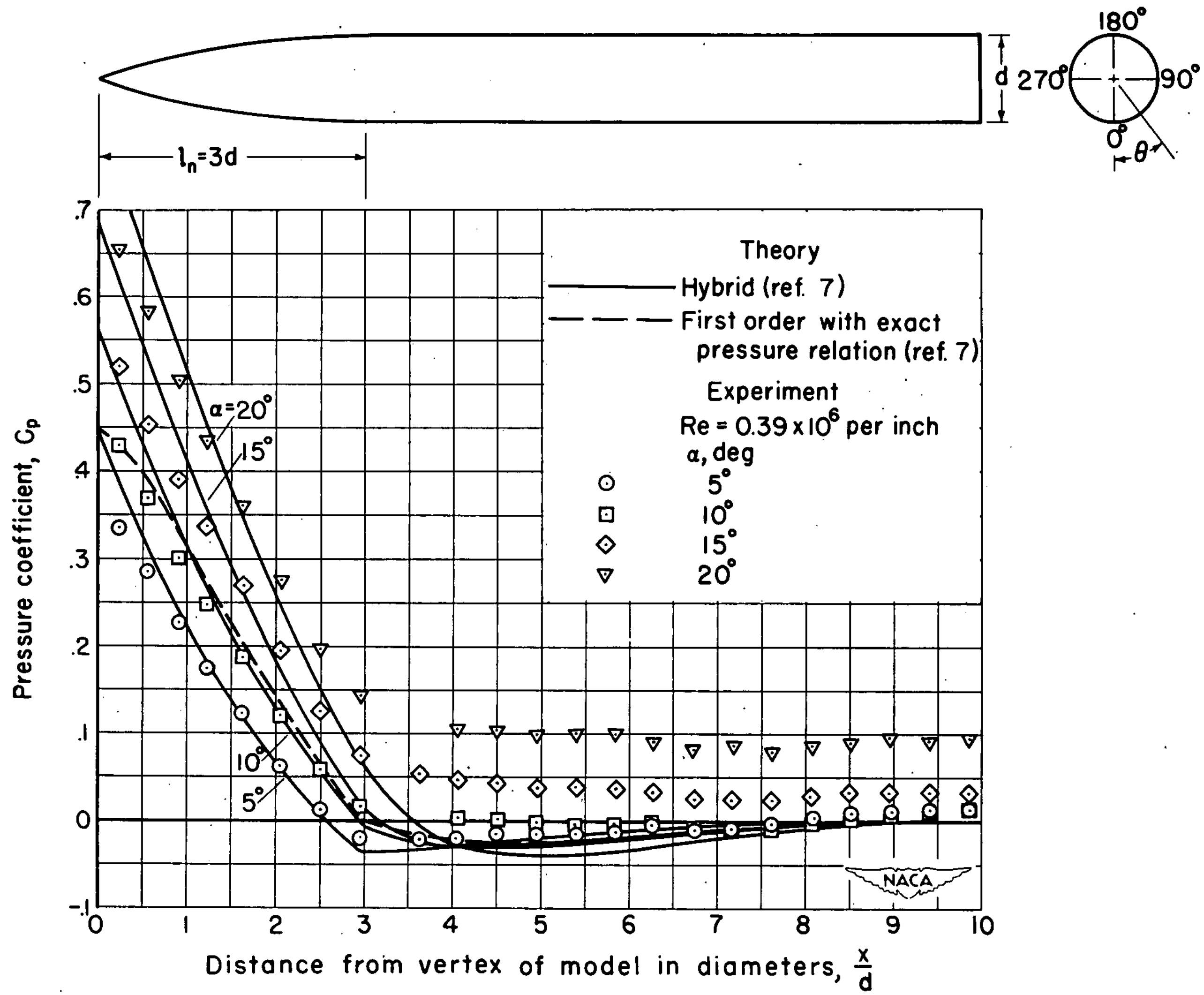

(b) $\theta = 30^{\circ}$

Figure 4.- Continued.

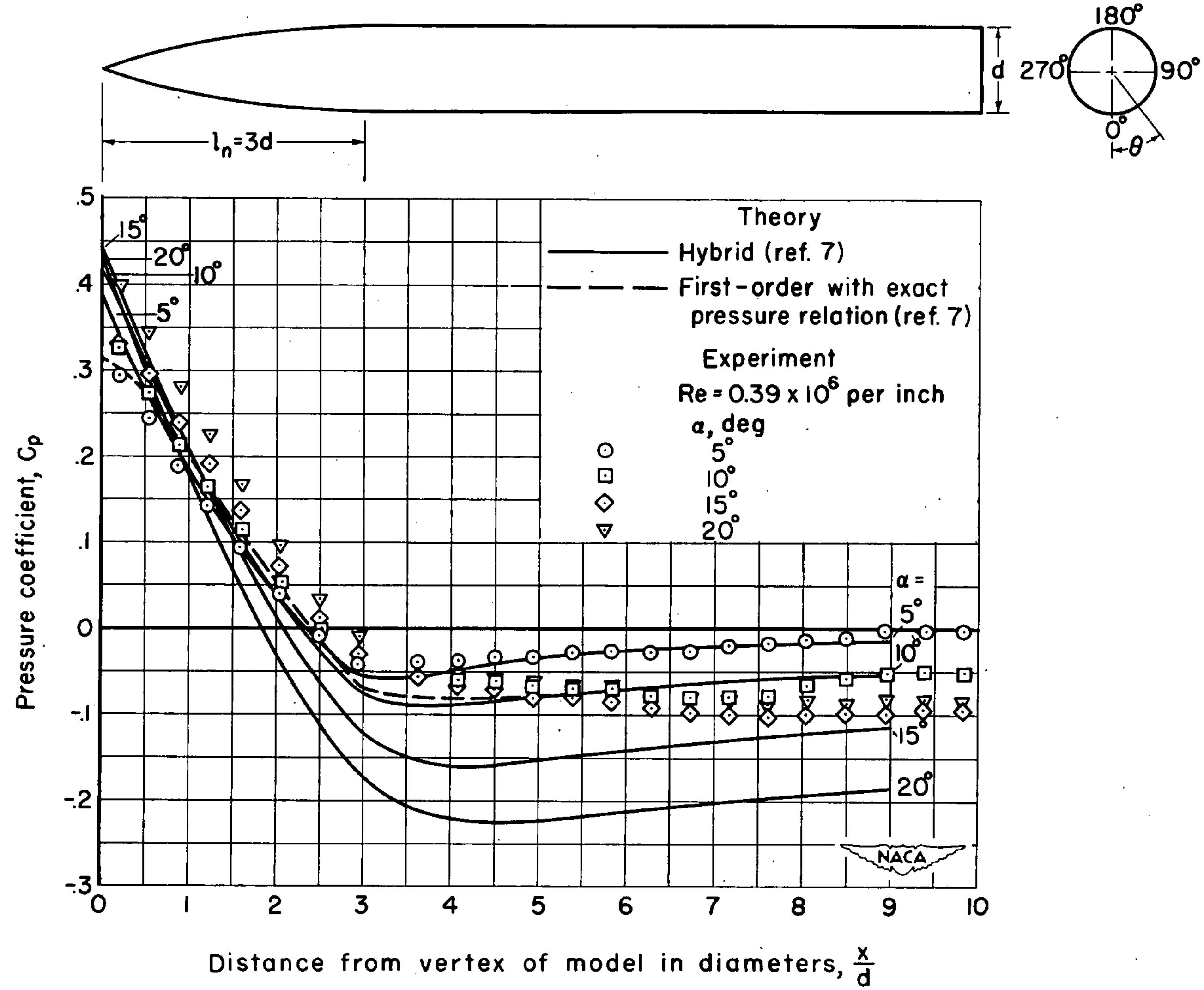

(c) $\theta = 60^{\circ}$

Figure 4.- Continued.

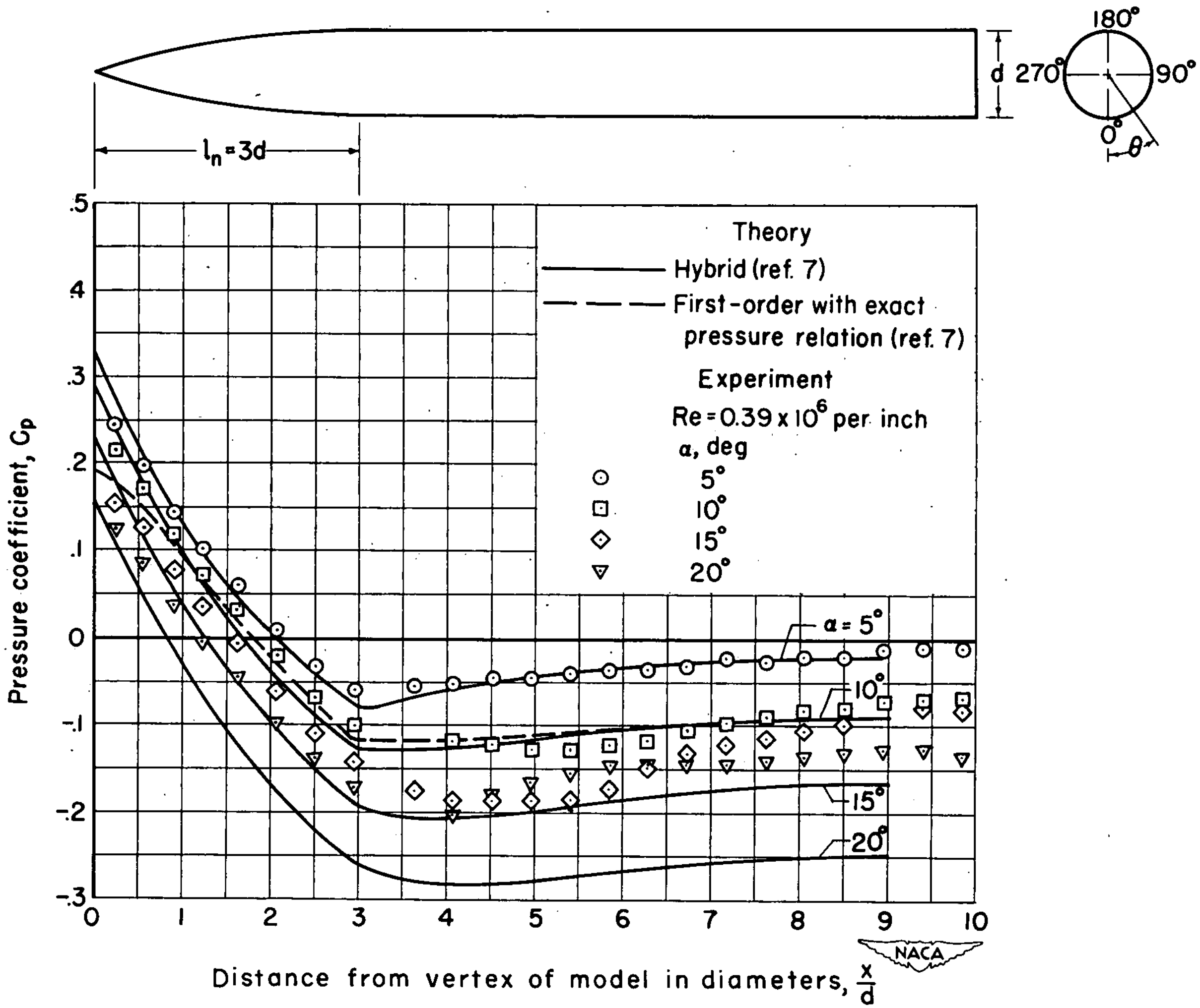

(d) $\theta = 90^{\circ}$

Figure 4.- Continued.

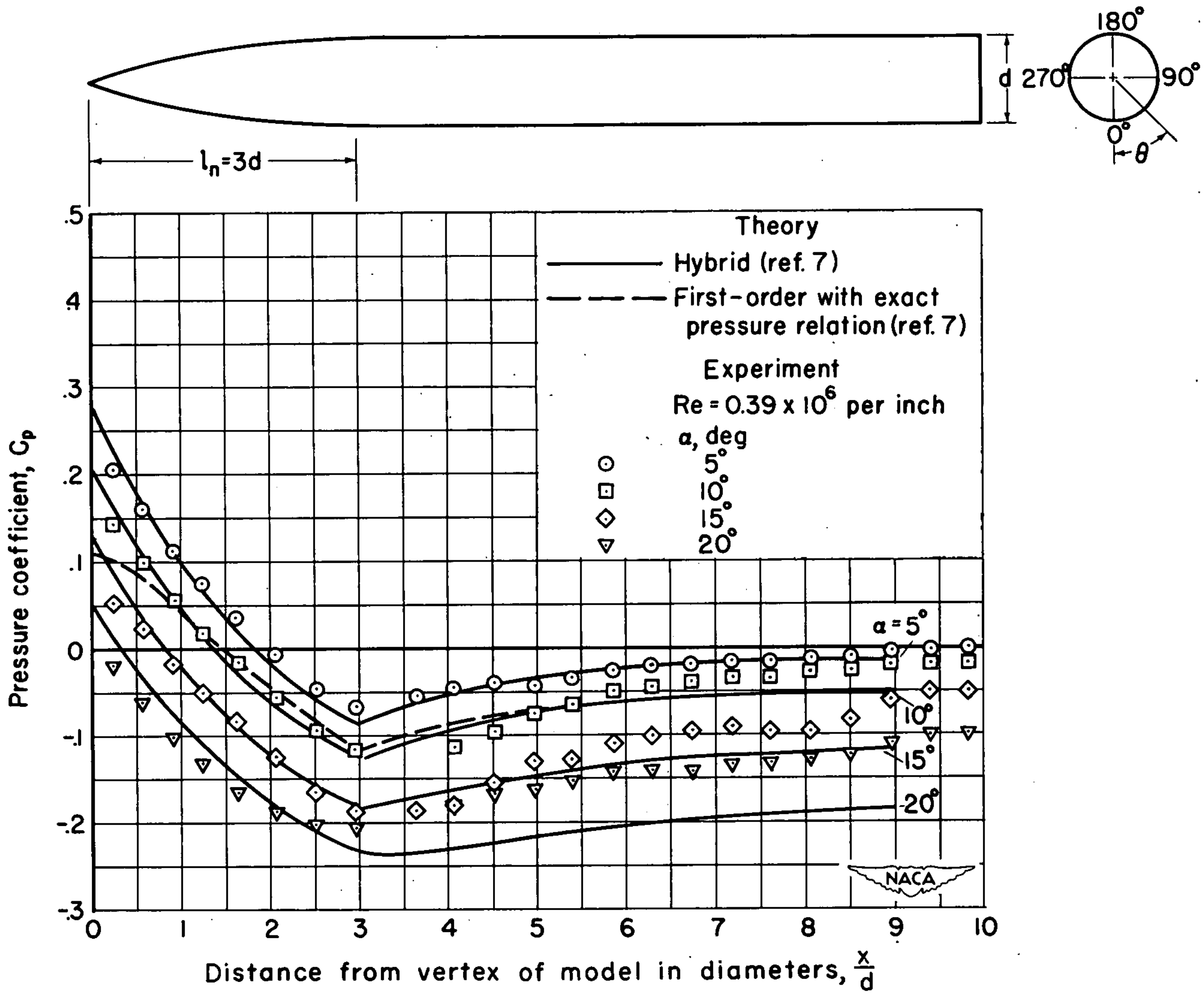

(e) $\theta = 120^{\circ}$

Figure 4.- Continued.

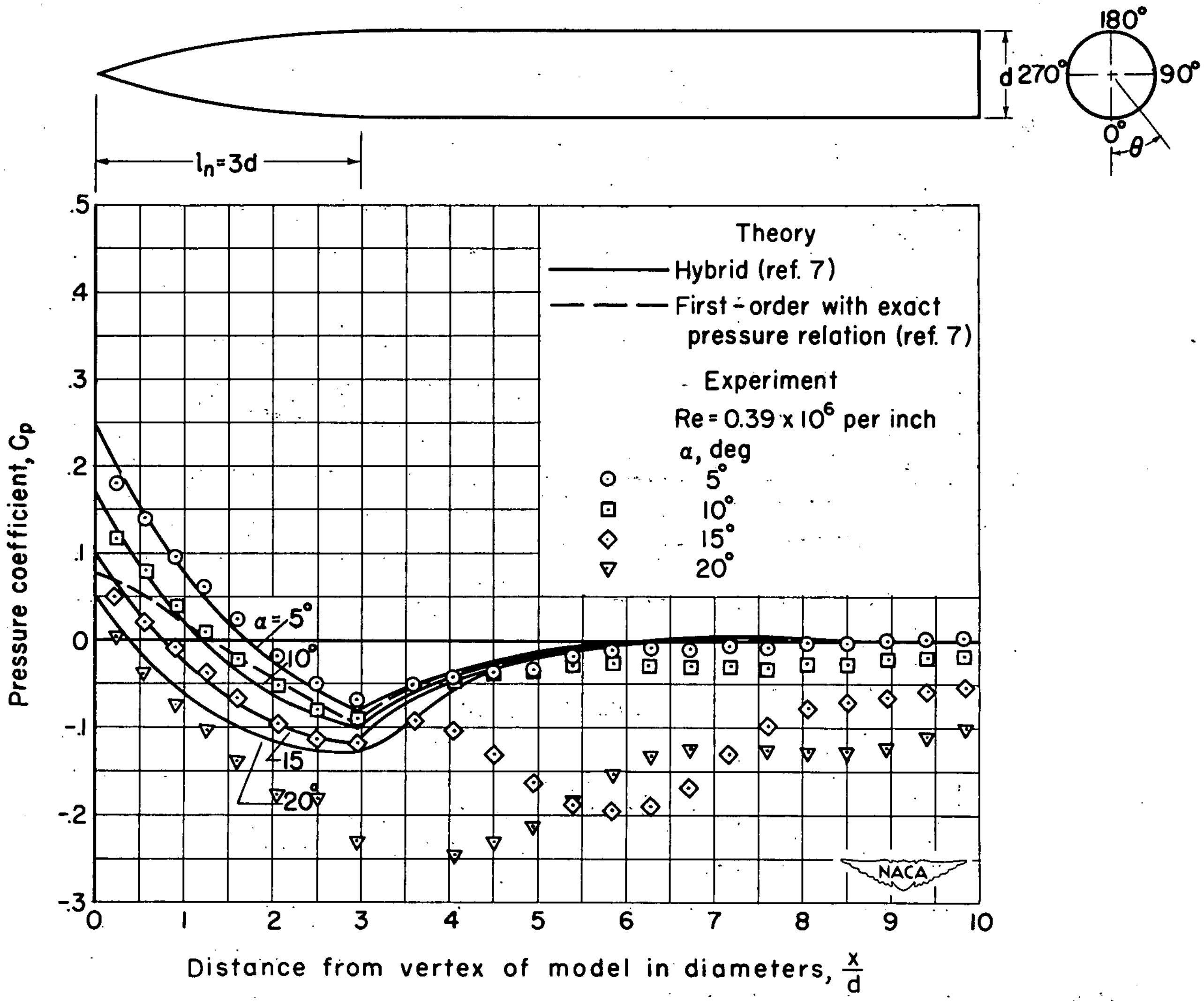

(f) $\theta = 150^{\circ}$

Figure 4.- Continued.

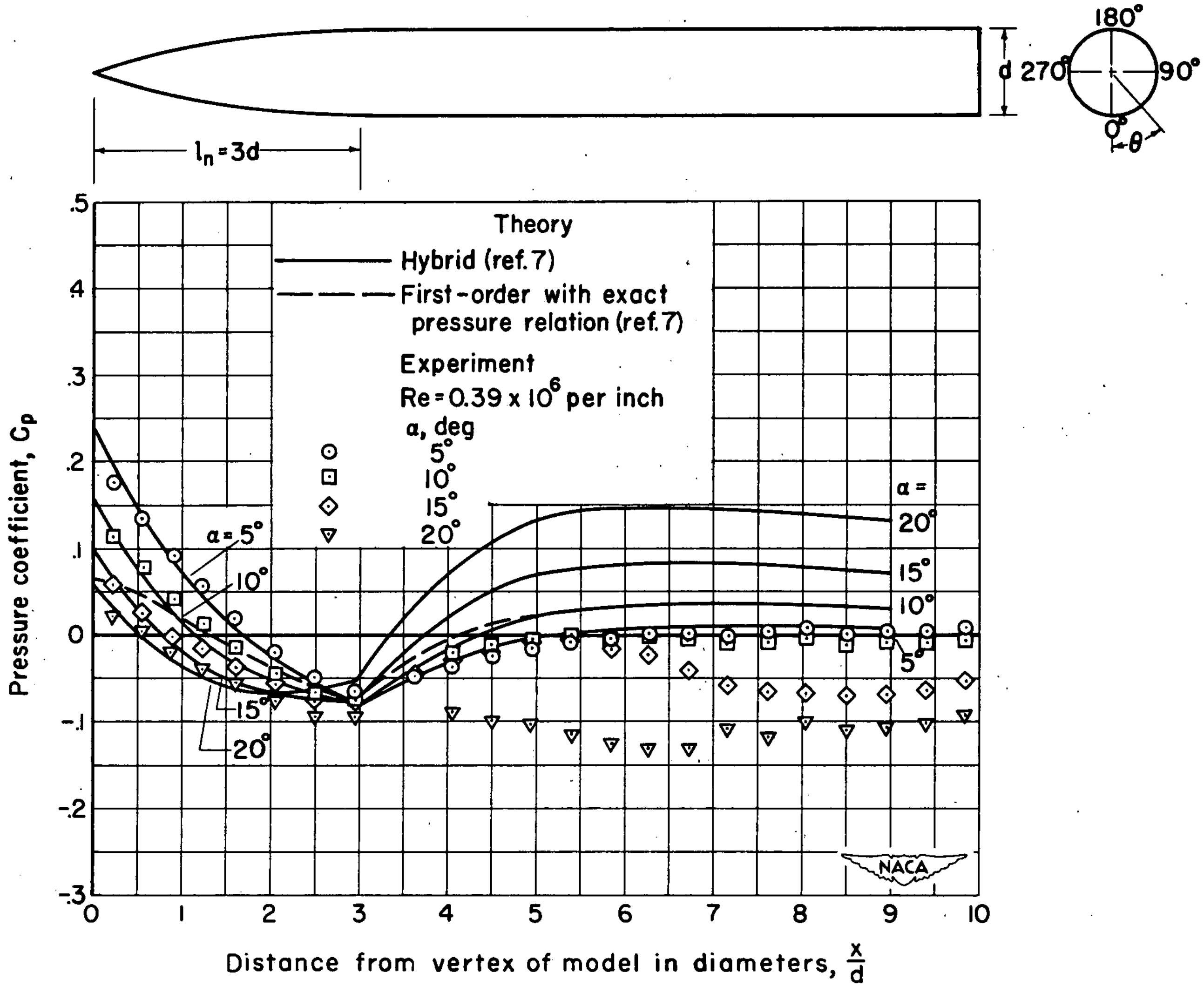

(g) θ = 180°

Figure 4.- Concluded.

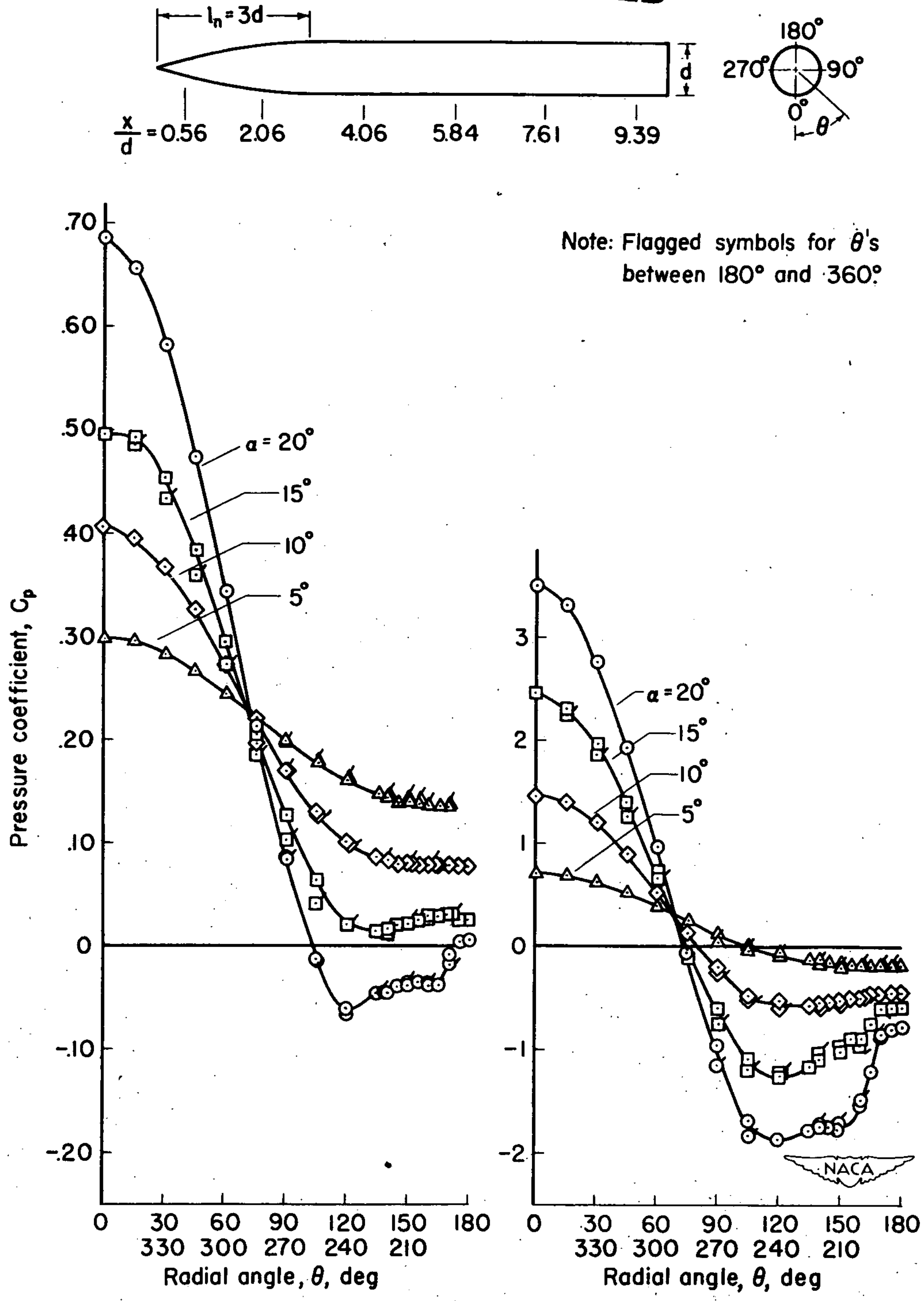

(a) $\frac{x}{d}$ = 0.56 (b) $\frac{x}{d}$ = 2.06

Figure 5.- Experimental circumferential pressure distributions at various angles of attack; $R_e = 0.39 \times 10^6$ per inch, $M_o = 1.98$.

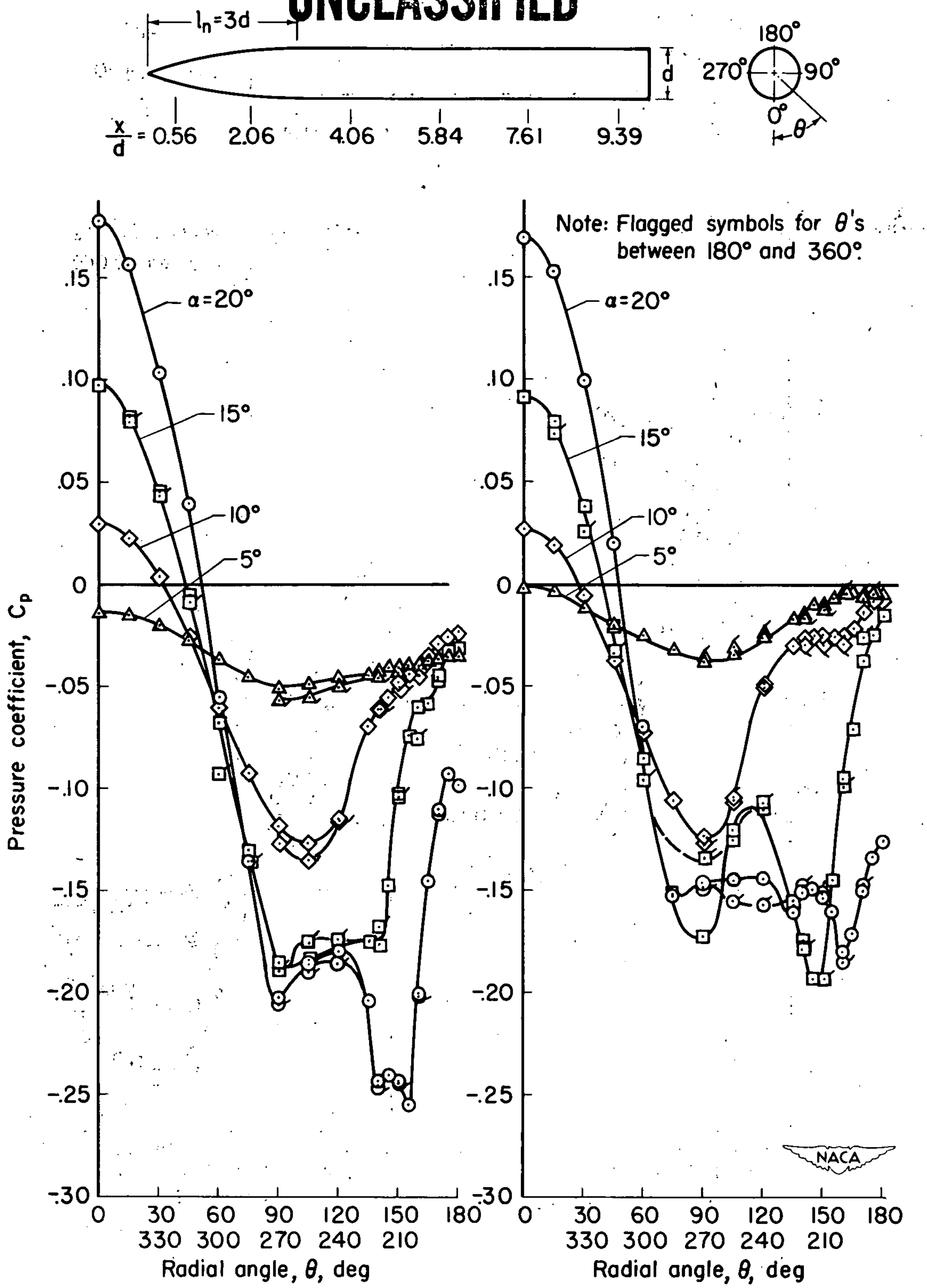

(c) $\frac{x}{d}$ = 4.06

(d) $\frac{x}{d}$ = 5.84

Figure 5.- Continued.

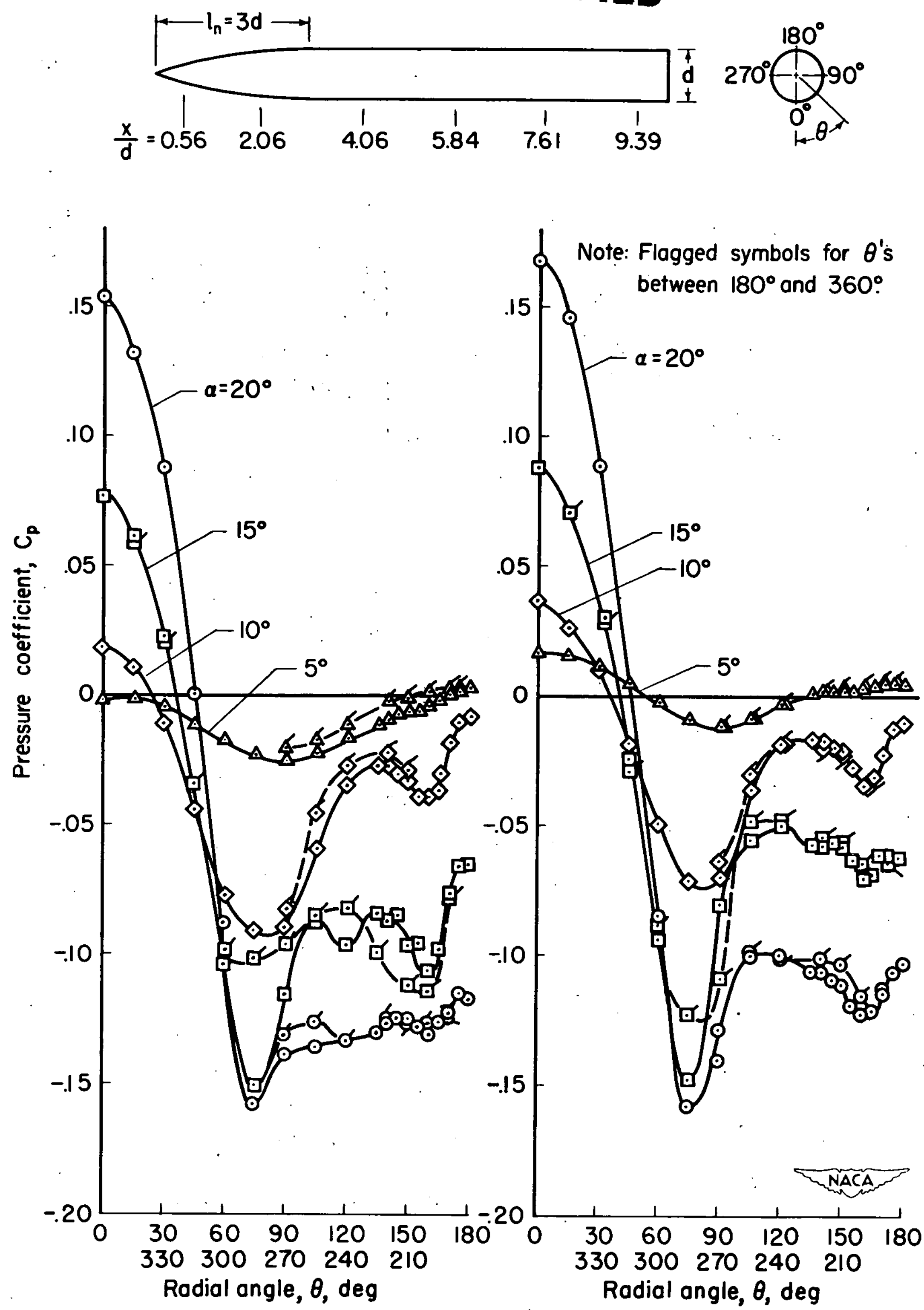

(e) $\frac{x}{d}$ = 7.61 (f) $\frac{x}{d}$ = 9.39

Figure 5.- Concluded.

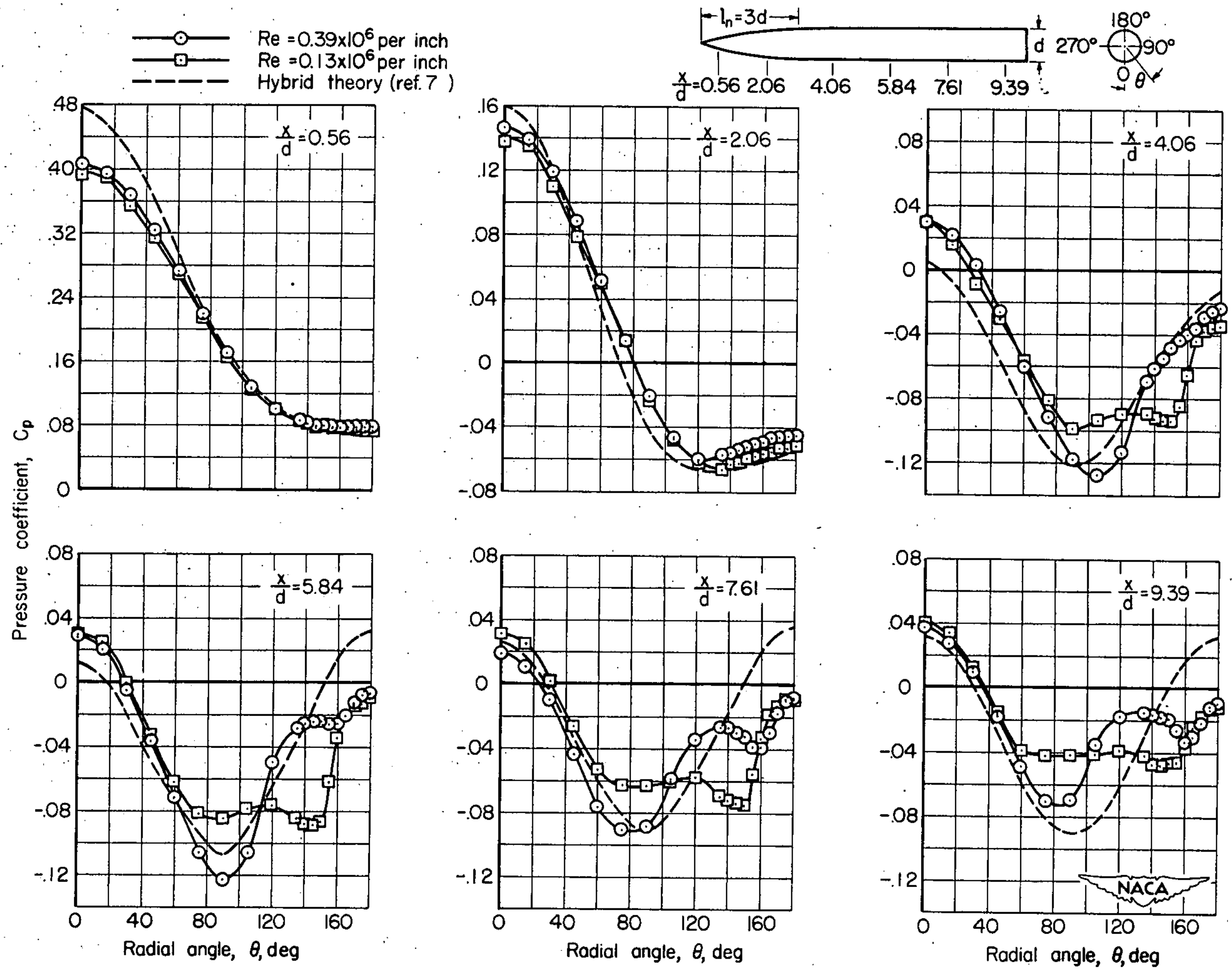

(a) $\alpha = 10^{\circ}$

Figure 6.- Effect of Reynolds number on the circumferential pressure distributions; $M_o = 1.98$.

UNCLASSIFIED

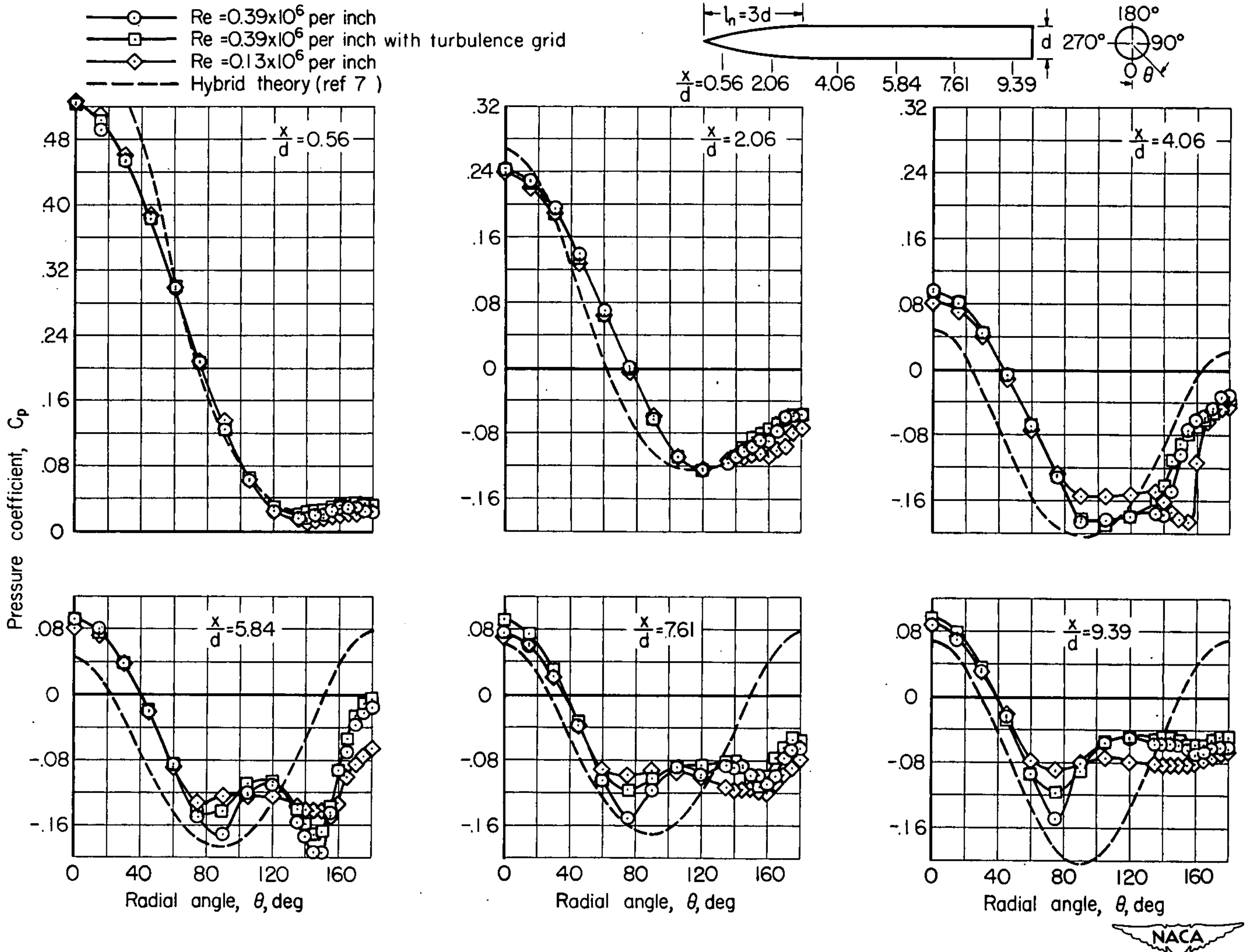

(b) $\alpha = 15^{\circ}$

Figure.6.- Continued.

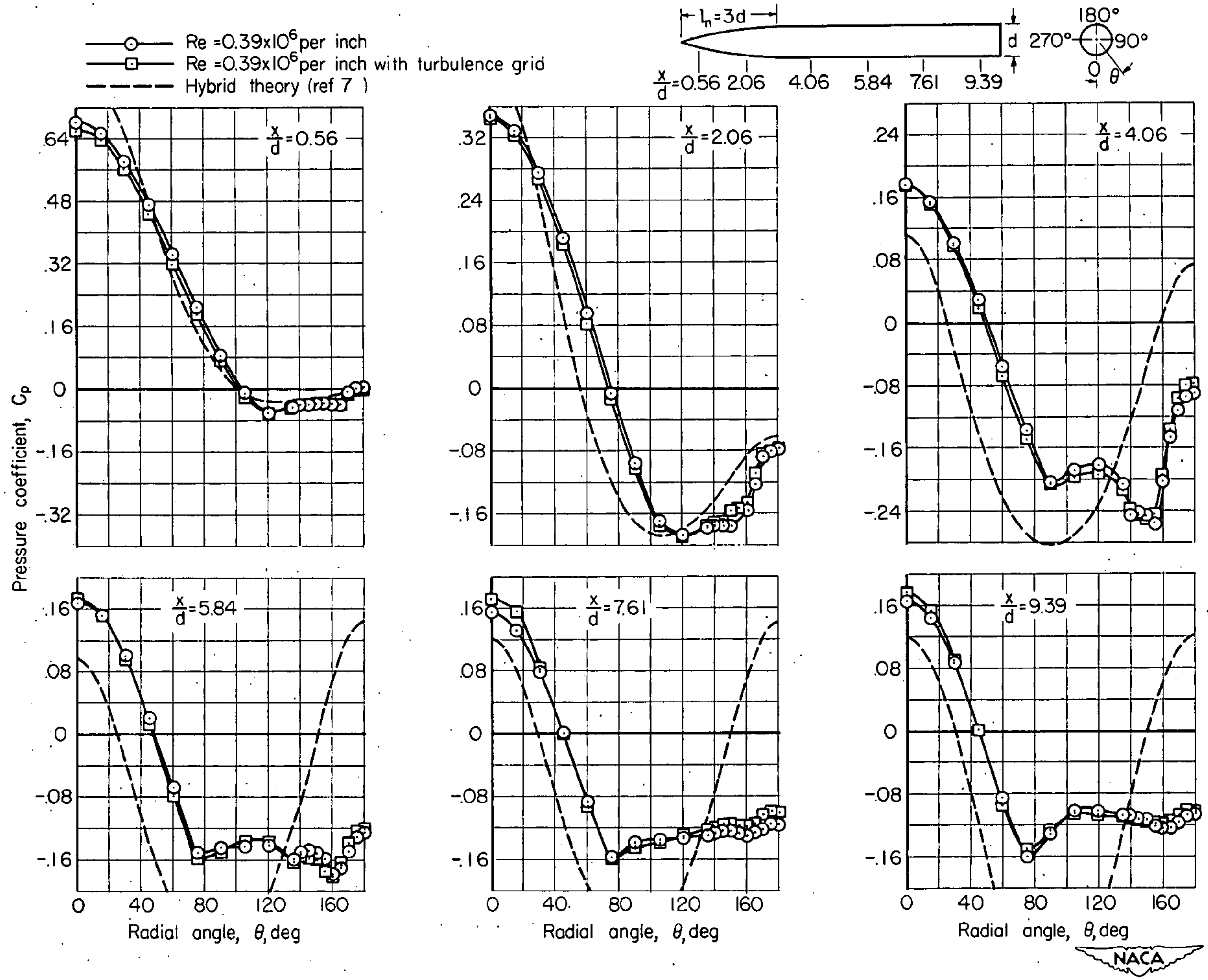

(c) $\alpha = 20^{\circ}$

Figure 6.- Concluded.

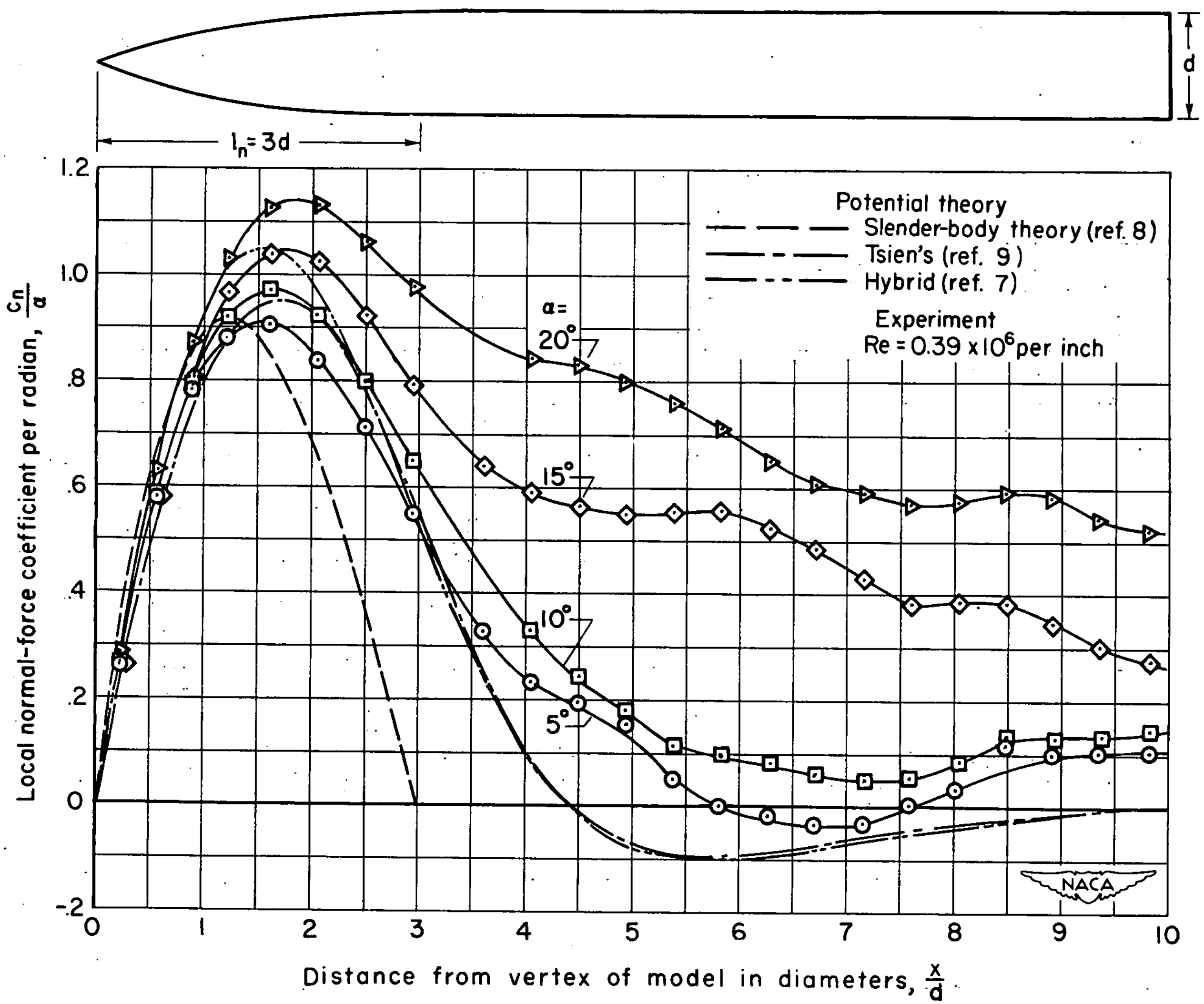

Figure 7.- Comparison at various angles of attack of the normal-force distributions determined by experiment and by potential theory; $M_o = 1.98$.

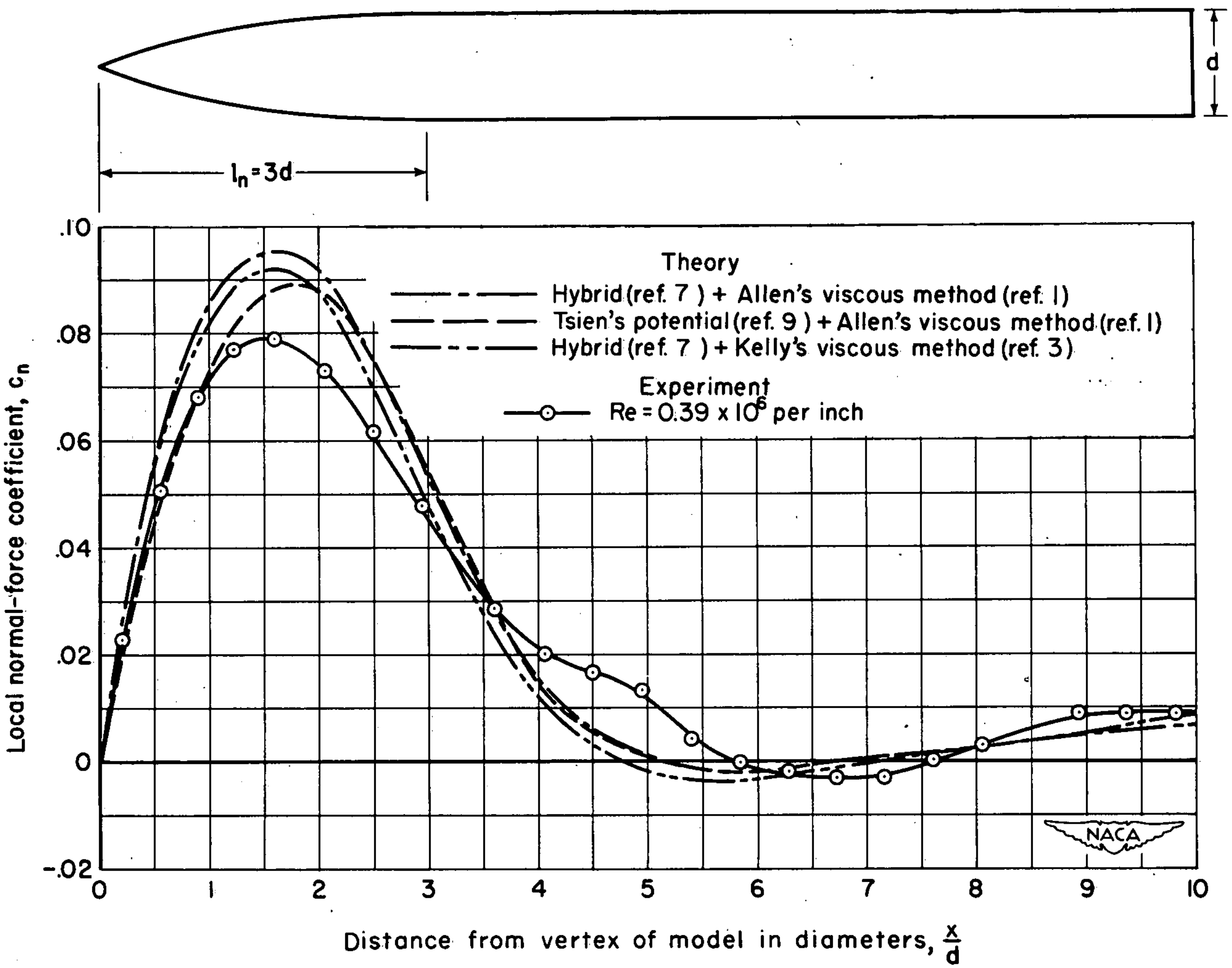

(a) $\alpha = 5^{\circ}$

Figure 8.- Comparison at various angles of attack of the normal-force distributions determined by experiment and by the theoretical methods of Allen and Kelly; $M_o = 1.98$.

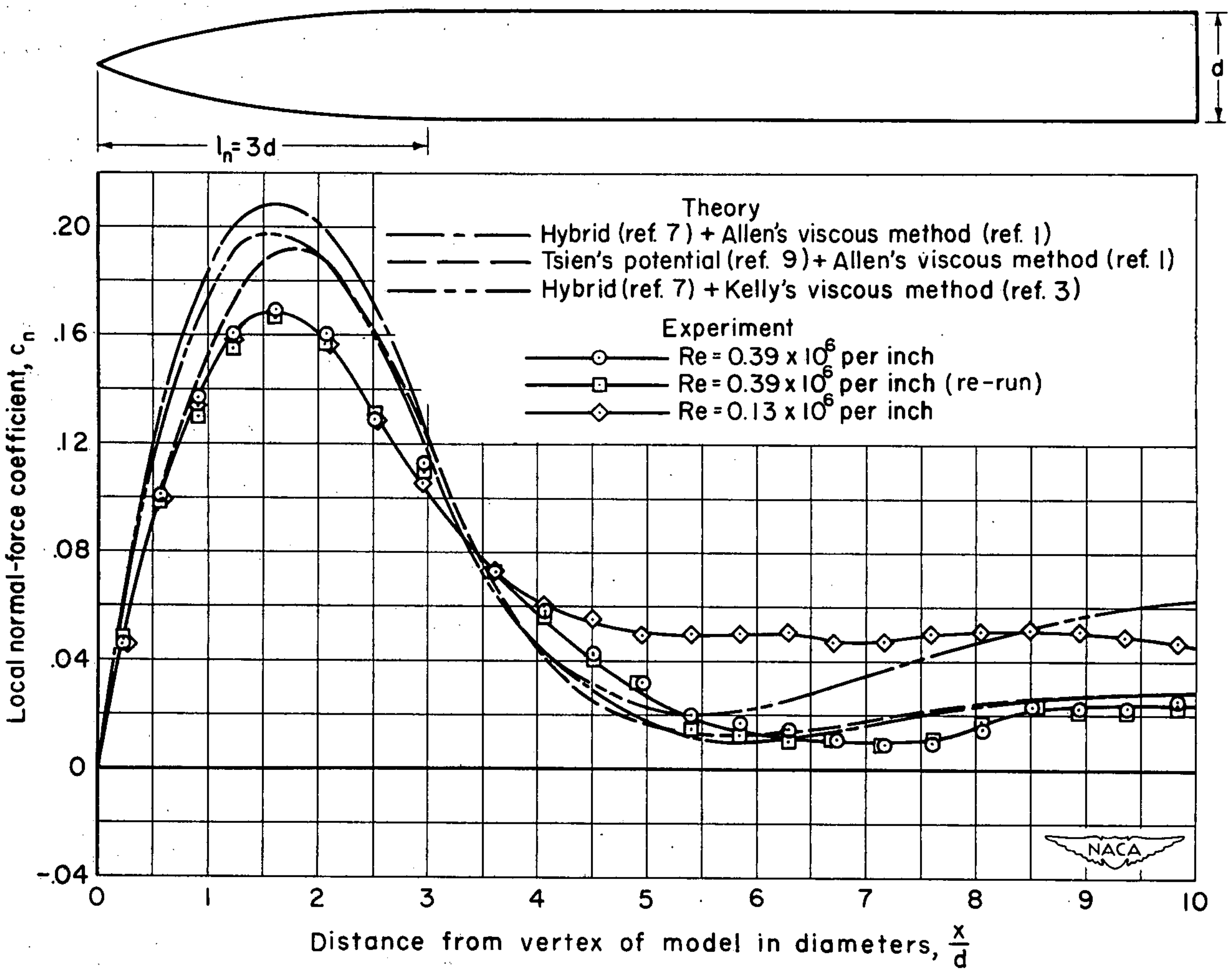

(b) $\alpha = 10^{\circ}$

Figure 8.- Continued.

UNCLASSIFIED

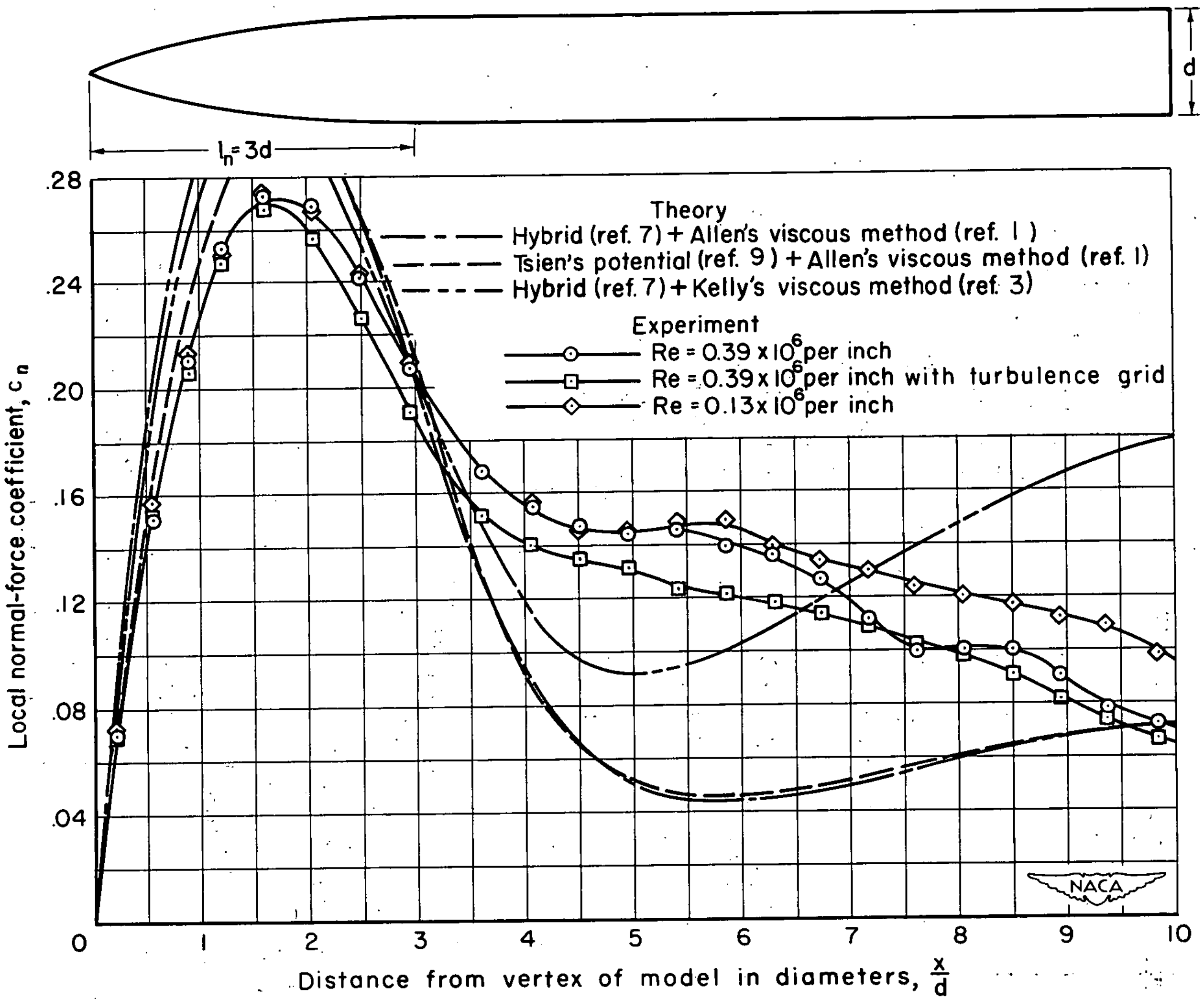

(c) $\alpha = 15^\circ$

Figure 8.- Continued.

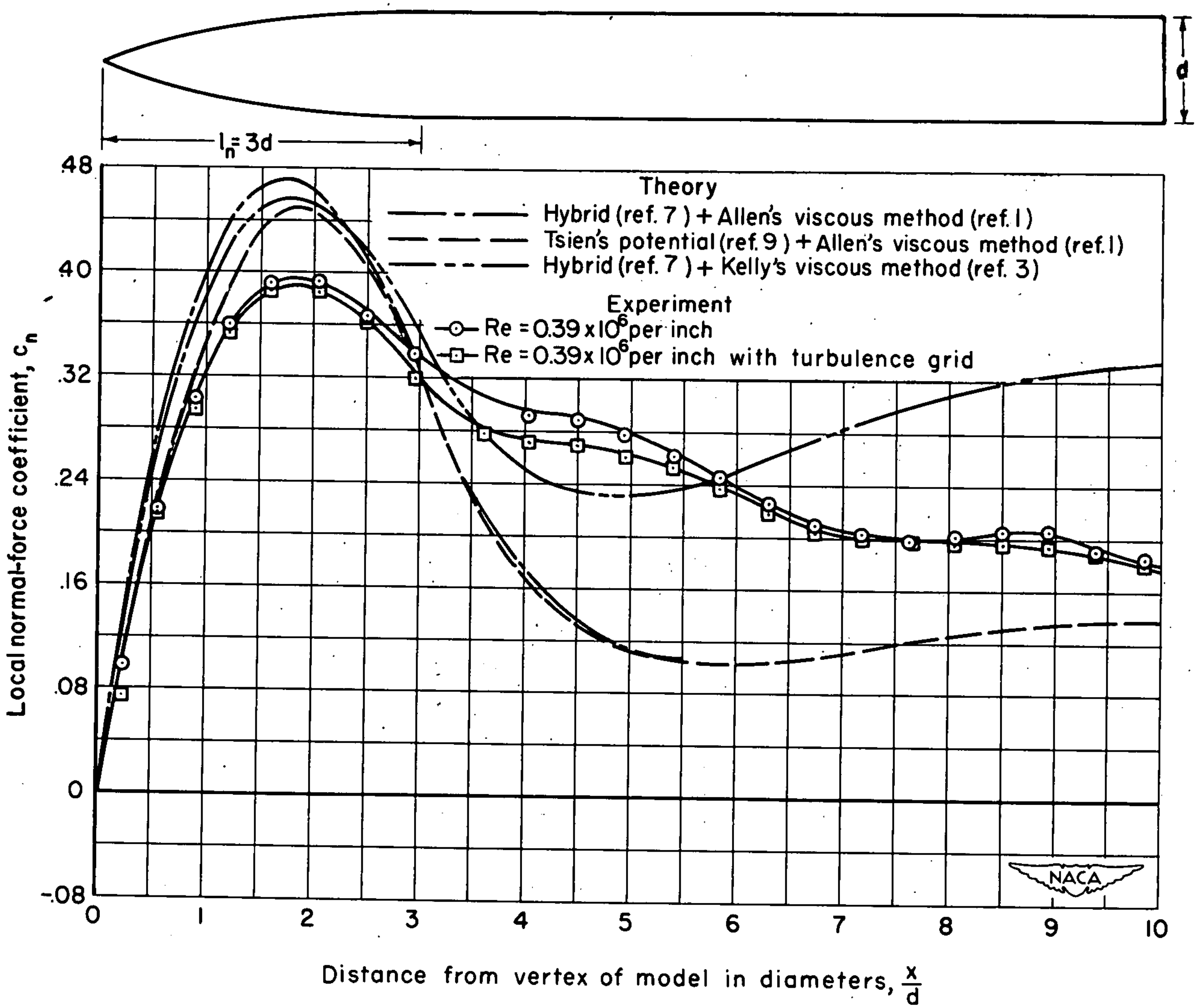

(d) $\alpha = 20^{\circ}$

Figure 8.- Concluded.

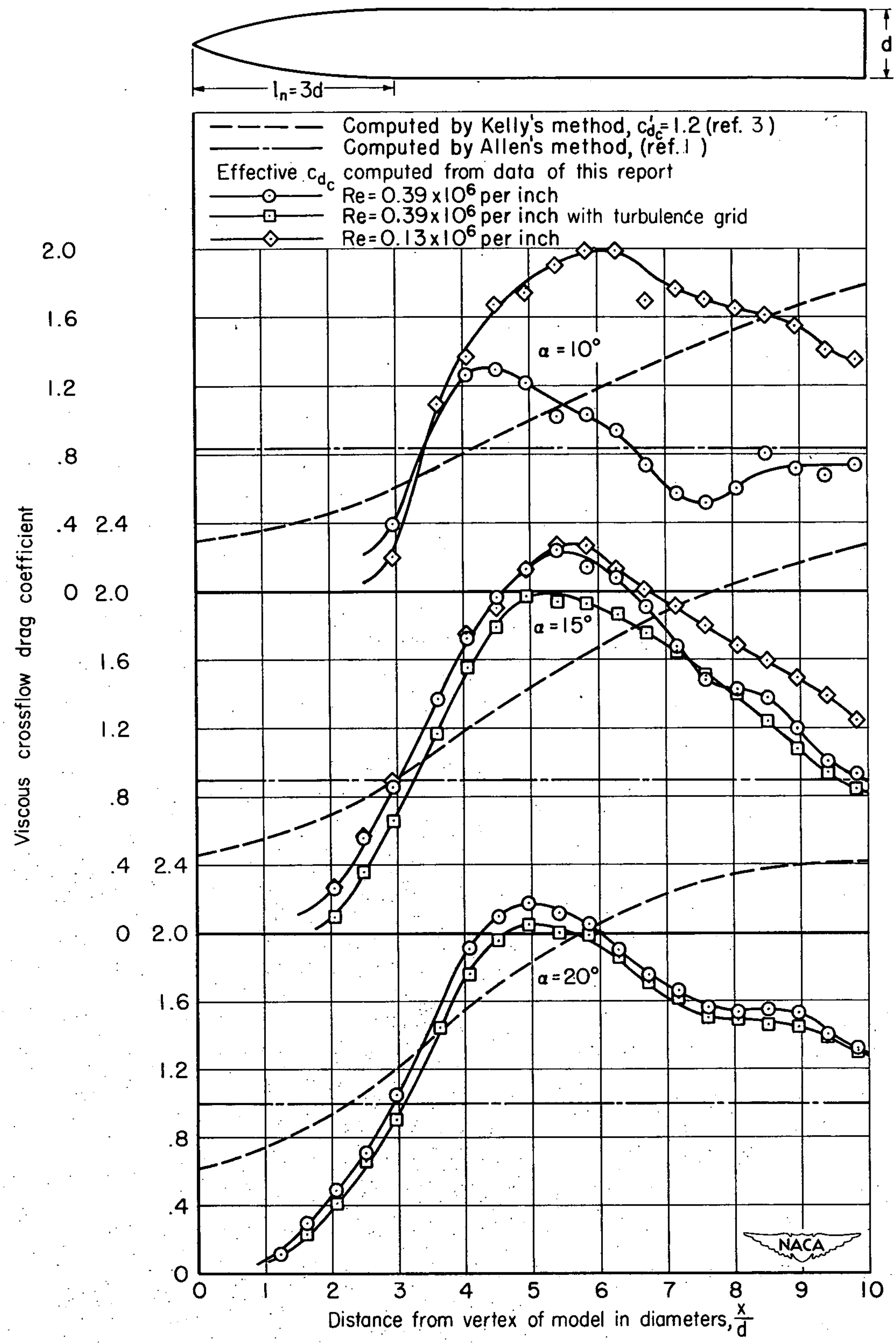

Figure 9.- Distributions of viscous crossflow drag coefficients; $M_o = 1.98$.

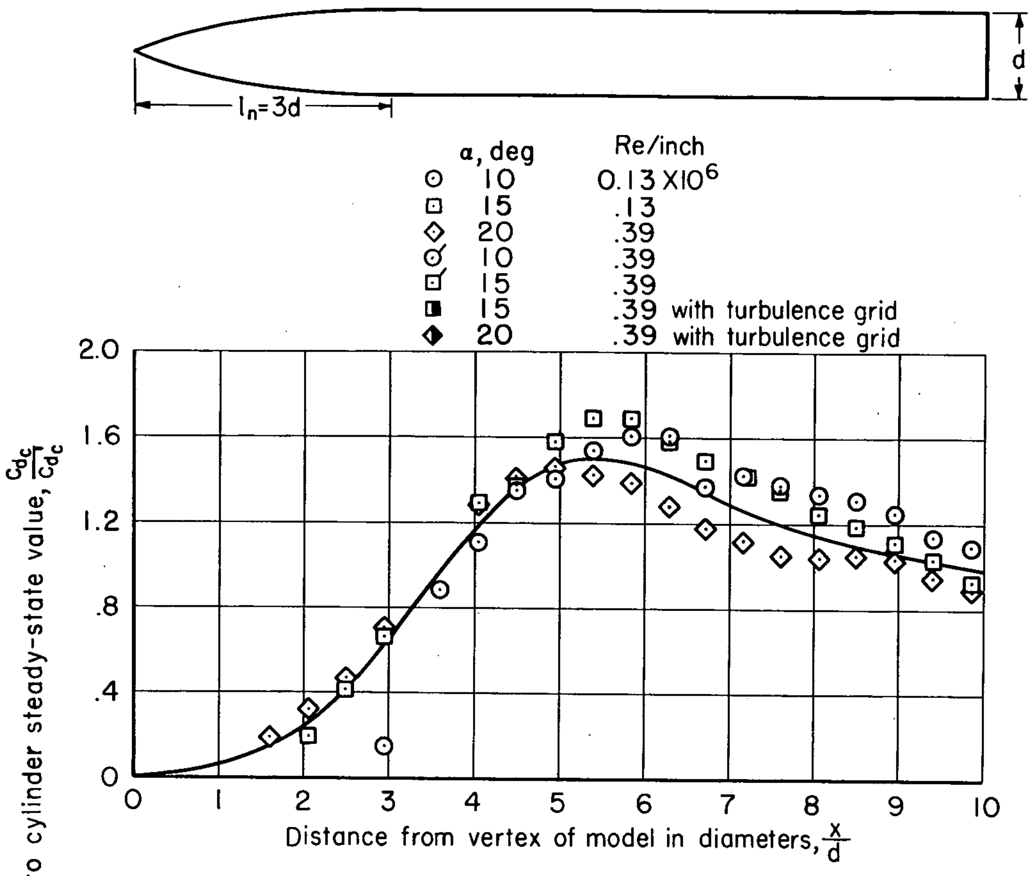

(a) Data for little or no Reynolds number effect.

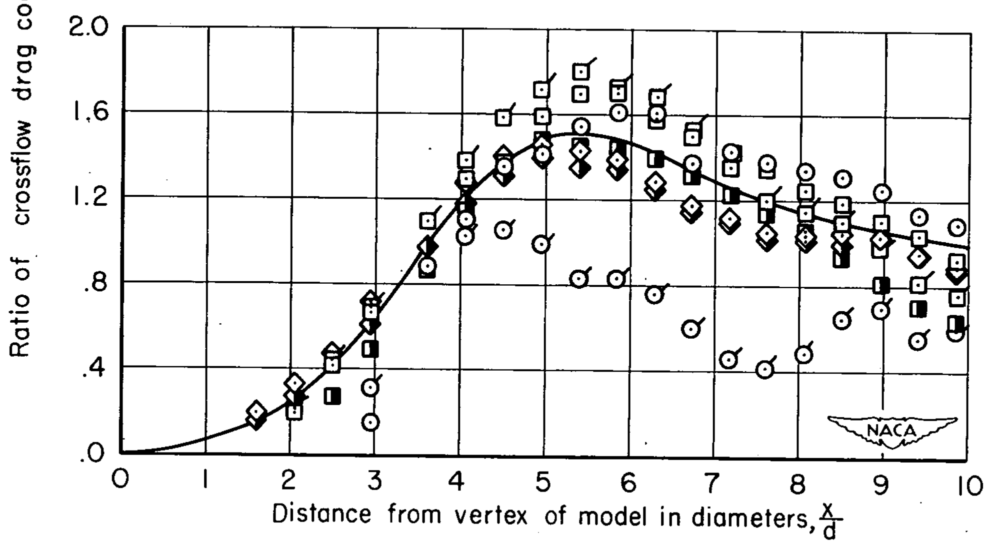

(b) All of the data.

Figure 10.- Correlation of distributions of crossflow drag coefficients; $M_o = 1.98$.

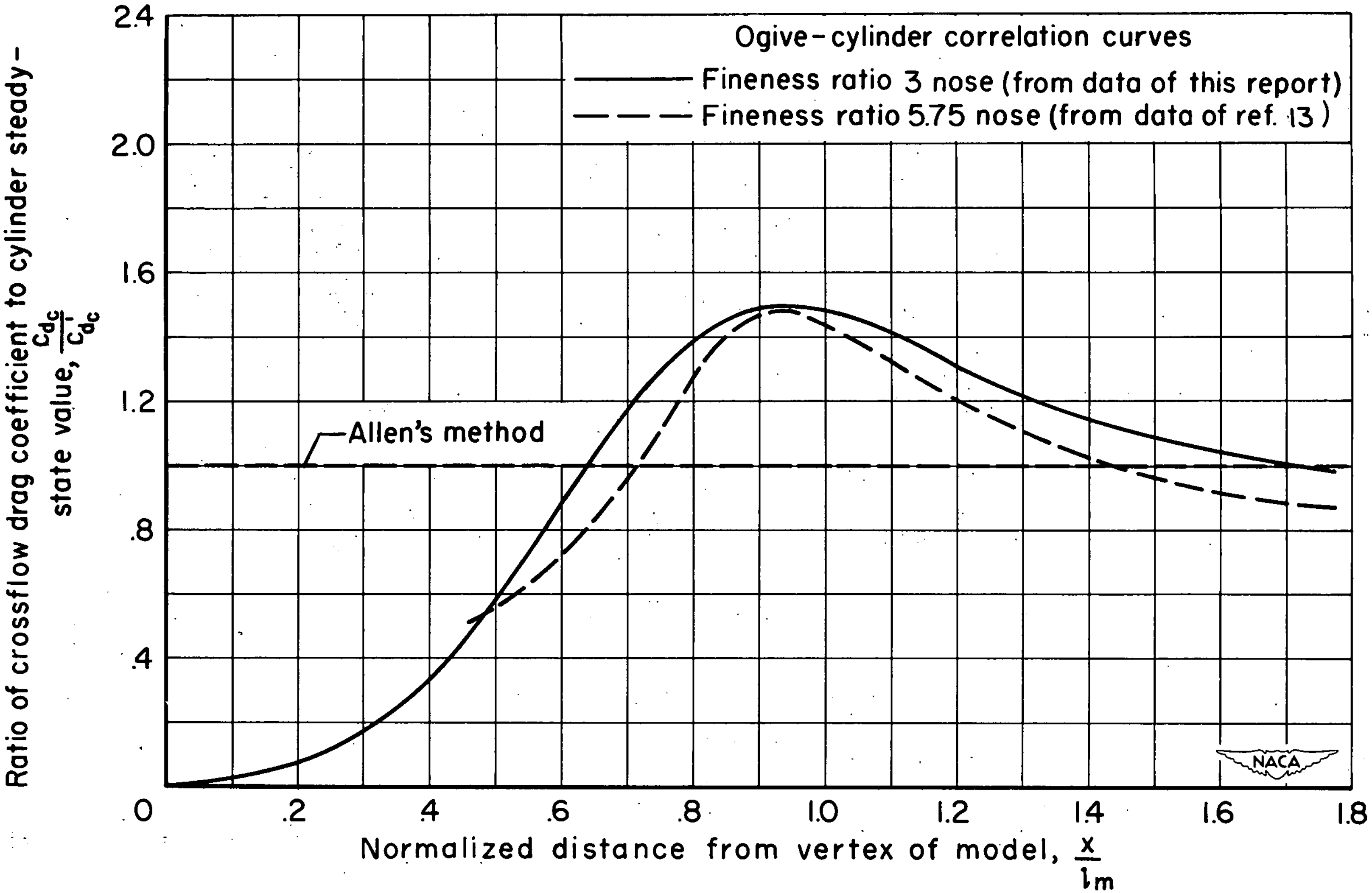

Figure 11.- Correlation of distributions of crossflow drag for two bodies; $M_o = 1.98$.

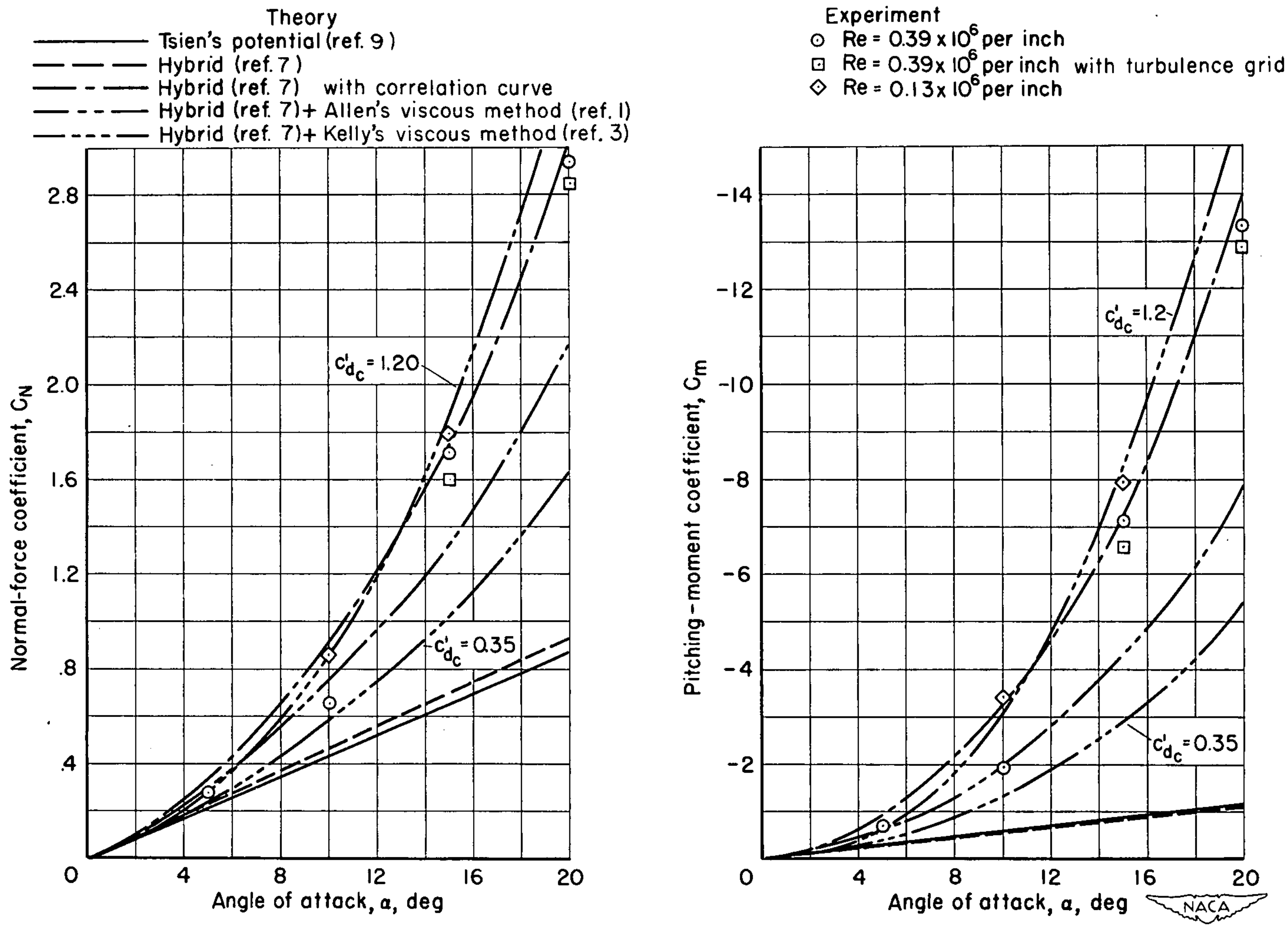

Figure 12.- Comparison of theoretical and experimental normal-force and pitching-moment coefficients; $M_o = 1.98$.

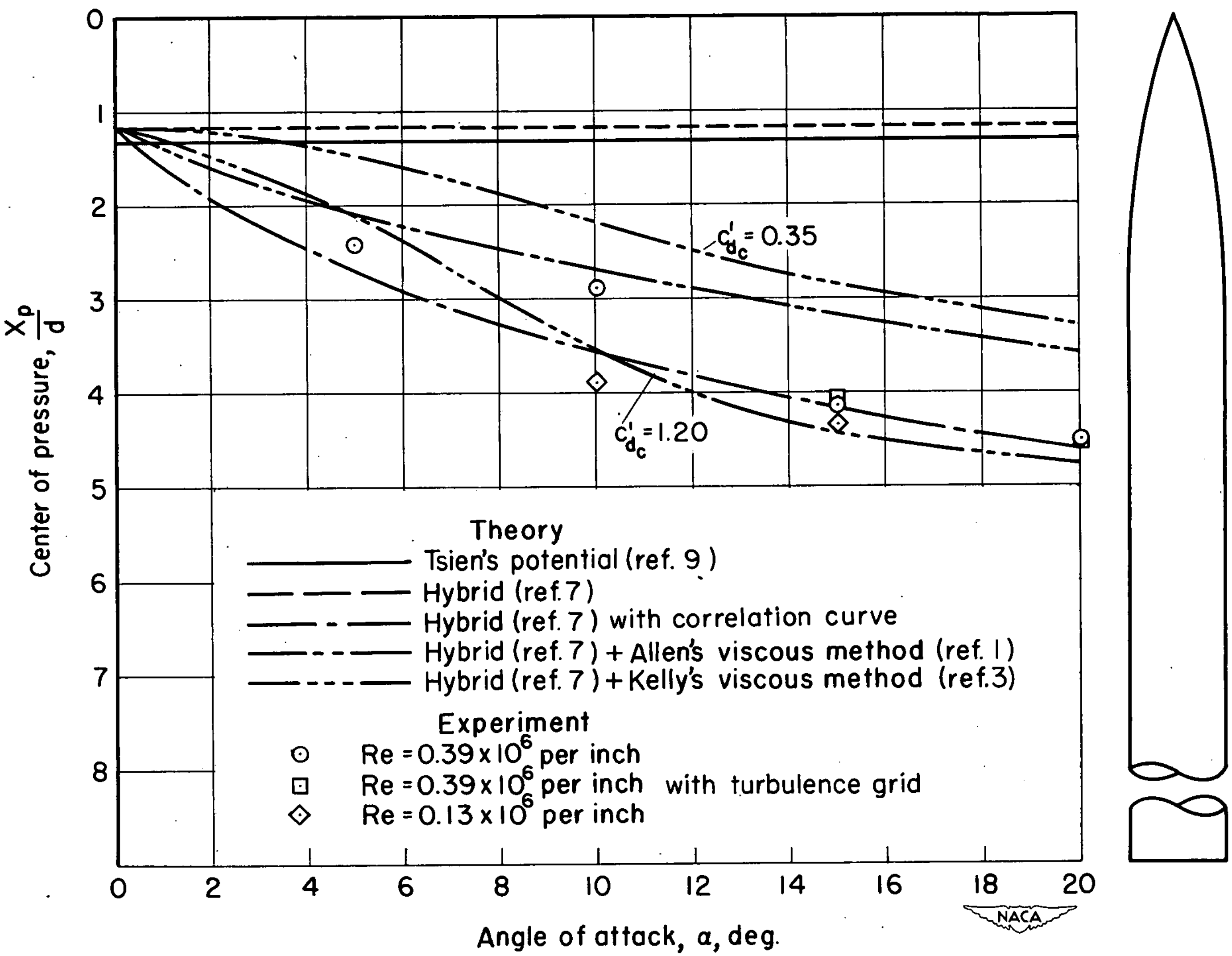

Figure 13.- Comparison of theoretical and experimental center-of-pressure locations.

UNCLASSIFIED

[redacted]

UNCLASSIFIED

[redacted]

UNCLASSIFIED

[redacted]